ENN Encyclopedia of Nanoscience and Nanotechnology
www.aspbs.com/enn

Carbon Nanotube–Based Inorganic Supramolecular Nanoassemblies

M. Bottini, M. I. Dawson, T. Mustelin

Burnham Institute for Medical Research, 10901 North Torrey Pines Road, La Jolla, CA 92037, USA

CONTENTS

1. Introduction
2. Coated Carbon NTs
3. Filled Carbon NTs
4. Conclusions
Glossary
References

1. INTRODUCTION

Nanotechnology is the science of manipulating and assembling matter on an atomic and molecular scale in order to develop novel materials with enhanced physical and chemical properties. One of the primary aims of nanotechnology is the fabrication of composites of nanoscale entities for use in multifunctional systems, including optoelectronics, sensing, and catalysis.

Among the nanomaterials recently introduced by nanotechnology, carbon nanotubes (NTs) have undergone the most intense investigation because of their extraordinary physicochemical properties [1]. While graphite and diamond are two allotropic forms of carbons, NTs belong to the family of fullerenes, which encompass the third allotropic form. NTs can be thought of as a graphene sheet rolled into a tubular structure and are structurally single-walled carbon nanotubes (SWNTs) or multi-walled carbon nanotubes (MWNTs). The former consists of a single graphene sheet, whereas the latter consists of many concentric and nested graphene sheets. Both categories are characterized by nanometric dimensions and a high aspect ratio (ratio between length and diameter). In this regard, SWNTs have diameters from 0.3 to 2 nm and lengths up to 1 μm [2], while the bigger MWNTs have diameters in the order of 100 nm and lengths from 1 to several microns.

MWNTs have been known for almost 50 years [3]. In fact, vapor-grown carbonaceous filaments were first described more than a century ago [4, 5]. As can happen for materials that *will* be important, they were not intentionally obtained but were industrial by-products in manufacturing coke. Early transmission electron microscope (TEM) images of MWNTs clearly revealed both tubular and "bamboo" internal morphologies despite the fact that the image resolution at that time was much lower. The first commercial TEM was put in the market by Siemens in the 1940s. The accurate determination of internal morphology required improved macroscopic and spectroscopic instrumentation [6, 7]. In 1991, Iijima reported the discovery of concentric MWNTs in the carbonaceous deposit formed on a cathode in an electric arc discharge reactor during the preparation of fullerenes and a detailed characterization [8]. During the last decade, scientists worldwide have enthusiastically and extensively studied MWNTs. Owing mainly to the fact that SWNTs are truly *nano*objects by having outer diameters that are more than one order of magnitude smaller than those of MWNTs, SWNTs are even object of greater scientific interest.

NTs have very interesting physicochemical properties such as ordered structure with high aspect ratios, light weight, high mechanical strength, high electrical conductivity, high thermal conductivity, metallic or semimetallic behavior, and high surface area. The combination of these properties makes NTs unique materials with the potential for applications in several fields as diverse as electronics, photonics, catalysis, and biomedicine. For instance, our and other research groups have been exploring the application of NTs in nanomedicine. By using the tools and knowledge of nanotechnology for biomedical purposes nanomedicine aims to preserve and improve health. This research may lead to the development of more effective means for delivering and targeting pharmaceutical, therapeutic, and diagnostic agents. The development of such nanotechnology-based agents involves the identification of specific cell and receptor target related to each clinical conditions and the appropriate nanocarrier to achieve the desired response with minimal adverse effects. NTs, owing to their extremely high aspect ratio, represent a potential multivalent scaffold for drug delivery and constructing nanoassemblies capable of binding many membrane receptors. Two main obstacles to utilization

ISBN: 1-58883-161-2

Encyclopedia of Nanoscience and Nanotechnology
Edited by H. S. Nalwa
Volume 12: Pages (153–177)

of nonfunctionalized (pristine) NTs in nanomedicine are their poor solubility under physiological conditions and tendency to form aggregates. To overcome these problems, NT surfaces have been functionalized by adsorption, electrostatic interaction, or covalent bonding processes. By the addition of appropriate molecules or chemical groups, the functionalized NTs become more hydrophilic and biocompatible, and aggregate less. Furthermore, recent toxicologic and pharmacokinetic studies indicate that functionalization improves their cytotoxicity profile (*in vivo*) and decreases uptake by the liver or other organs of the reticuloendothelial system. These results suggest that functionalized NTs can be used in nanomedicine more efficiently than nonfunctionalized (pristine) NTs and other nanomaterials. However, the batch production of NTs with uniform structural and chemical characteristics, high quality control, and minimal impurities remains a challenge that limits their development for this purpose.

In many cases NTs must be attached to, or filled with, other molecules, macromolecules, and nanoparticles (NPs) to fabricate nanodevices or composites capable of taking full advantage of their unique properties. In fact, the resulting nanocomposites can have properties that drastically differ from those of each individual component.

Nanocomposites can be fabricated by such strategies as covalent or noncovalent decoration of pristine (p) or acid-oxidized (ox) NT sidewalls with preformed NPs, or by the *in situ* growth of NPs onto NTs. The choice of a specific technique for decorating NTs with NPs is usually dictated by the final application of the nanocomposite. For instance, because NT-based electronic devices must retain the extraordinary electronic properties of NTs, *in situ* growth or noncovalent functionalization of pristine NTs is the preferred strategy. Covalent functionalization of oxNTs is not recommended because oxNTs are produced by oxidation in strong acids that also destroys the high aspect ratio of NTs and dramatically changes their electronic properties. For each carboxyl group introduced onto an NT an equal number of π electrons are removed from its conjugated π system. Covalent functionalization is recommended for NT-based nanoassemblies having biomedical applications, because these NTs are mainly used as scaffold. The oxidation process used for their formation has cut them into short "nanopipes" of suitable length, namely few hundred nanometers, for fabricating intracellular carriers of NPs. In contrast, the energies leading to noncovalent functionalization of NT sidewalls with NPs would be too weak to guarantee the mechanical stability necessary to assemble a delivery system.

The choice of the linker between NTs and NPs is also dictated by the application of the nanoassembly. For instance, in biomedical applications NTs that are easily visualized by simple optical microscopy are useful. Therefore, the NPs should be fluorescent and the linker used to couple them to the NT sidewall should not quench their fluorescence caused by interacting with the NTs, which would provide a nonirradiative decay pathway for the photoexcited electrons of the NPs. For NT-based photoelectrochemical cell fabrication, the linker should permit electron transfer from the excited states of the NP (luminophore) into the conduction band of the NT (quencher).

NT filling can provide interesting applications such as containers for nanosized catalysts with delayed action or as *nano*needle delivery devices. NTs partially filled with short nanorods or NPs of a catalyst could be used in catalytic processes. No chemical reaction will take place as long as the graphene shell is present to prevent the catalyst from contacting the reactants. Under oxidizing conditions, the protective integrity of the graphene shell would be disrupted to allow access to the catalyst. Fullerenes encapsulated into SWNTs exhibit such novel properties as coalescence under prolonged exposure to an electron beam and diffusion. The latter property could permit the use of NTs as *nano*needles and have many applications as carriers. Biologically active molecules (or atoms) could be attached to fullerenes for delivery to a specific tissue, cell type, or an intracellular compartment. Encapsulation of endofullerenes (fullerenes encapsulating foreign atoms) into NTs might have exciting applications in radiography and scintigraphy by facilitating the transport of heavy elements or radio elements to a highly localized area.

In this chapter, we address the supramolecular assembly of both SWNTs and MWNTs with metallic, semiconducting, insulating, and magnetic NPs. We describe both the decoration of the external sidewall and the filling of the inner cavity. While traditional organic synthesis involves the making and breaking of covalent bonds to construct a desired molecule, generally speaking, supramolecular chemistry refers to the area of chemistry which focuses on the noncovalent bonding interactions of molecules to assemble molecules, macromolecules, and NPs into complexes. These far weaker and reversible noncovalent interactions include hydrogen bonding, metal coordination, hydrophobic forces, van der Waals forces, π–π interactions, and/or electrostatic effects. In particular, the layer-by-layer technique has been widely used for the deposition of NPs onto both macroscopic substrates and spherical colloids. Although the supramolecular assembly of NPs onto NT sidewalls in aqueous solvents is limited owing to the hydrophobic nature of pristine NTs, polymer wrapping permits the functionalization of NTs through noncovalent attachment of molecules and produces individually dispersed NTs in aqueous solutions. In this case NT–polymer interactions are thermodynamically preferred over NT–water interactions, and the hydrophobic surface of the NTs is suppressed.

2. COATED CARBON NTs

2.1. Metallic NPs

Recently, interest in the decorating of NTs with metallic NPs has increased for three main reasons. First, optoelectronic devices could take advantage of the coupling between the plasmonic modes of metal NPs and the plasmons of NTs. Second, their high aspect ratio, large surface area, and unique electronic properties make NTs excellent scaffolds for such catalysts as Pt, Pd, and Rh, which have been used in electrochemical and fuel cells. Third, NTs have been used as scaffolds for metal NPs for use in hydrogen storage and for biological, biochemical, and chemical applications as sensors.

Strategies developed to fabricate supramolecular nanoassemblies of NTs and metallic NPs can be divided into two main groups: (1) decoration with previously grown NPs, and (2) *in situ* growth of NPs onto NTs.

2.1.1. Decoration of Carbon NTs with Previously Grown Metallic NPs

Although this section presents the techniques used to decorate both pristine (p) and oxidized (ox) NTs with Au NPs (GNPs), similar techniques have been used to link other metallic NPs to NTs.

Pristine Carbon NTs pNT-GNP nanoassemblies have been made using linkers that were either hydrophobically anchored or adsorbed *via* π–π stacking interactions onto the sidewalls of pNTs. Ellis *et al.* [9] reported the connection of octanethiol (OT)-capped GNPs to pNTs by hydrophobic interactions (Fig. 1). Acetone molecules were first adsorbed onto the imperfections of the pNT sidewalls through C=O···C interactions or resonance structures, so that the acetone methyl groups studded the pNT surface. OT-capped GNPs were then anchored onto the pNTs through hydrophobic interdigitation between the acetone methyl groups and the OT octyl chains to achieve a self-assembled molecular (SAM) layer capping the GNPs. Interdigitation between adjacent GNPs adsorbed onto the pNTs avoided the coalescence of the GNPs and resulted in wire-like structures consisting of large polycrystals [10]. The distance between GNPs could be modulated by adjusting SAM chain length and structure and, in turn, could modulate quantum effects (e.g., single-electron hopping and Coulomb blockade) to enable the molecular-level design of nanodevices for switching, sensing, and information storage.

Polycyclic aromatic molecules have been observed to adsorb onto pNT sidewalls through π–π stacking interactions [11–13]. Their adsorption has been exploited as a method to decorate pNTs with macromolecules, silica NPs, and organometallic molecules. Mono- and polycyclic aromatic ring-terminated alkylamines [2-phenylethylamine, *N*-(1-naphthyl)ethylenediamine and 1-pyrenemethylamine] have been used by Ou *et al.* [14] as linkers for fabricating NT-GNP nanoassemblies. The surface of GNPs was covered by the ω-aryl alkylamines through interaction of the nitrogen lone electron pairs. The modified GNPs were subsequently adsorbed onto pNT sidewalls *via* π–π stacking interactions between the terminal aromatic rings of the alkylamine linkers and the pNT surface (Figs. 2(A)–2(C)). The level of loading in the NT-GNP nanoassembly was monitored by UV–Vis absorption and photoluminescence spectroscopies. The vibronic absorption features of the aromatic rings were perturbed upon complexation of the linker onto the GNPs indicating strong interactions between the π-electron clouds of the aromatic rings and the plasmon electrons of the GNPs. The vibronic absorption features of the aromatic rings were further perturbed upon adsorption of the modified GNPs onto the pNT sidewalls. The surface plasmon resonance (SPR) absorption band of the GNPs was also perturbed upon complexation indicating interparticle plasmon coupling between GNPs that were in close contact. In general, the absorbance spectrum can give information about a system composed of colloidal GNPs. According to Zhong *et al.* [15], the position of the SPR absorption band depended upon particle size, interparticle distance, and the interaction of GNPs with other molecules in a colloidal dispersion. Thus, a red shift of the SPR band was attributed to interparticle plasmon coupling, a phenomenon observed even when just a few GNPs were clustered. This red shift in the plasmon of GNPs deposited onto pNTs suggested that the GNPs were densely packed on the NT surface. Finally, quenching of the photoluminescence of the aromatic rings upon complexation of the GNPs and pNTs indicated electron transfer (ET) between the aromatic rings (donor) and the two nanoassembly components (pNT and GNP), which functioned as quenchers.

Spectroscopic analyses were used by Liu *et al.* [16] to study the decoration of pNTs with GNPs to which 12-[4-(1-pyrenyl) butoxy]dodecanethiol (PBT) had been linked through thiol group–GNP interaction followed by adsorption of its pyrenyl groups onto the pNT surface (Fig. 2(D)). The fluorescence of PBT was quenched moderately by its binding to the pNTs and almost totally quenched through the further binding of GNPs, suggesting ET from the linker and the pNTs as well as from the GNPs. Moreover, the authors observed an enhanced Raman response. The two main contributions to the surface increase of Raman scattering of NTs on metallic surfaces occur through "electromagnetic" and "chemical" mechanisms [17]. The former is caused by an increase in

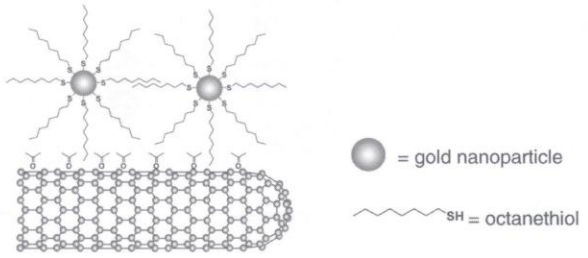

Figure 1. Decoration of pristine carbon NTs with octanethiol-capped gold NPs using acetone as a linker [9].

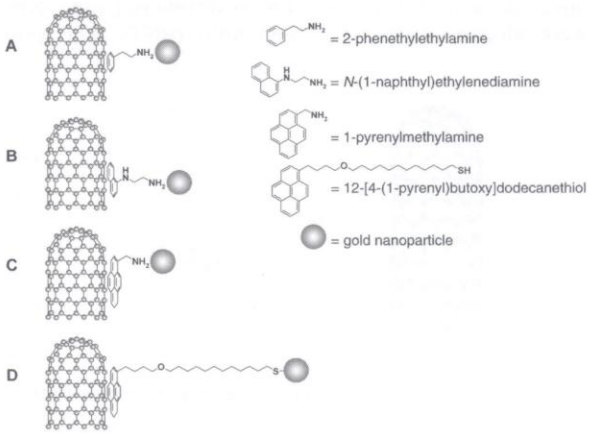

Figure 2. Decoration of pristine carbon NTs with gold NPs using polycyclic aromatic ring-terminated alkylamines linkers [14, 16].

the electromagnetic field at or near the metallic surface, and the latter is caused by ET between the metallic surface and the NTs and strongly depends on the NT electronic structure. Therefore, an observed increase in the Raman response suggests ET between the GNPs and the pNTs through the linker.

Oxidized Carbon NTs Functionalization of oxNTs usually employs the carboxylic groups produced by oxidation. Liu *et al.* [18] first reported an acid-based multireactant procedure assisted by cross-flow filtration and sonication to obtain open-ended and carboxylated short NTs which were termed pipes.

In a subsequent study, Jiang *et al.* [19] reported that negatively charged GNPs could be noncovalently attached to oxidized MWNTs using a polyelectrolyte as an electrostatic bridge (Fig. 3). First, MWNTs were oxidized by suspension in a concentrated sulfuric acid–nitric acid mixture (3:1 v/v) followed by sonication. FT-IR analysis indicated that the acidic oxidation introduced four types of functionality onto the MWNTs, namely hydroxyl ($3424\,cm^{-1}$), carboxyl ($1719\,cm^{-1}$), carbonyl ($1626\,cm^{-1}$), and sulfate ($1384\ cm^{-1}$) groups. The oxMWNTs were coated with a cationic polyelectrolyte [poly(diallyldimethylam monium chloride), PDAC] that ad-sorbed onto the NT surface because of the electrostatic interactions between the negative carboxate groups and the positive tetraalkylammonium groups. Finally, negatively charged GNPs were anchored onto NT surface through electrostatic interactions between the positively charged polyelectrolyte and the GNPs. The resulting NT-GNP structure showed quite uniform decoration of the GNPs onto the NT walls and ends that corresponded to the location of the functional groups. In this regard, this technique could represent an excellent method for monitoring the presence of negatively charged functional groups on the surface of NTs.

Kim *et al.* [20] reported using a similar procedure to decorate oxNTs with positively charged GNPs (Fig. 4). The latter were prepared by the phase transfer technique reported by Gittins *et al.* [21]. MWNTs were chemically functionalized by oxidation using ultrasonication in concentrated sulfuric acid–nitric acid (3:1 v/v) for 1–8 h. The authors showed that only NTs treated longer than 4 h were colloidally stable in aqueous media for at least 24 h. Positively charged GNPs were electrostatically deposited onto oxNTs that were negatively charged by deprotonation of the carboxylic acid groups introduced during chemical oxidation (Fig. 4(a)). Alternatively, positively charged GNPs were anchored onto negatively charged oxNTs fabricated depositing first the positively charged polyelectrolyte PDAC then a negatively charged polyelectrolyte poly(sodium 4-styrenesulfonate) (PSS) onto oxNTs (Fig. 4(b)). In this case, the density of the GNPs on the NTs was higher than that achieved by directly anchoring positively charged GNPs onto oxNTs. The authors rationalized that the higher loading was achieved by the polyelectrolyte coating that increased the number of negatively charged sites.

2.1.2. In Situ Growth

Many researchers have reported the *in situ* growth of metallic NPs onto NTs. The most common technique used to decorate NTs with noble metal NPs, especially in fuel cell applications, has been by reducing noble metal salts to metals in the presence of oxidized NTs [22–24] or pristine NTs with the aid of a surfactant or Nafion [25–28]. Other techniques are electrochemical deposition [29, 30], electroless deposition without reducing agents [31], substrate-enhanced electroless deposition (SEED) [32], intermittent microwave irradiation [33], water-in-oil nanoemulsion [34], supercritical carbon dioxide [35], and a surfactant-wrapping technique [36, 37], all of which are described below.

Electrochemical Deposition Quinn *et al.* [29] reported the electrodeposition of noble metals (Au, Pt, and Pd) under direct potential control onto the sidewalls of SWNTs that act as a nonsacrifical template for the growth of metal clusters (Fig. 5). The authors found that the size of the metal clusters increased significantly as the potential of the Ti electrode was made more negative and that, for a given nucleation potential, the cluster size increased with deposition time and metal salt concentration.

Electroless Deposition without Reducing Agents Choi *et al.* [31] reported the spontaneous formation of Au and Pt NPs onto the sidewalls of SWNTs when the latter were immersed in the corresponding metal salt solutions. The reported process differed from traditional electroless deposition in that no reducing agents or catalysts were required. The highly selective metallic NP deposition onto the SWNTs resulted

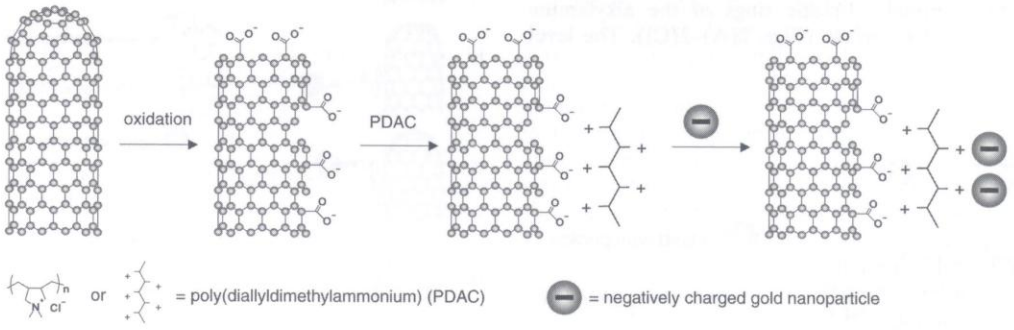

Figure 3. Decoration of oxidized carbon NTs with gold NPs using a cationic polyelectrolyte [poly(diallyldimethylammonium chloride), PDAC] as a linker [19].

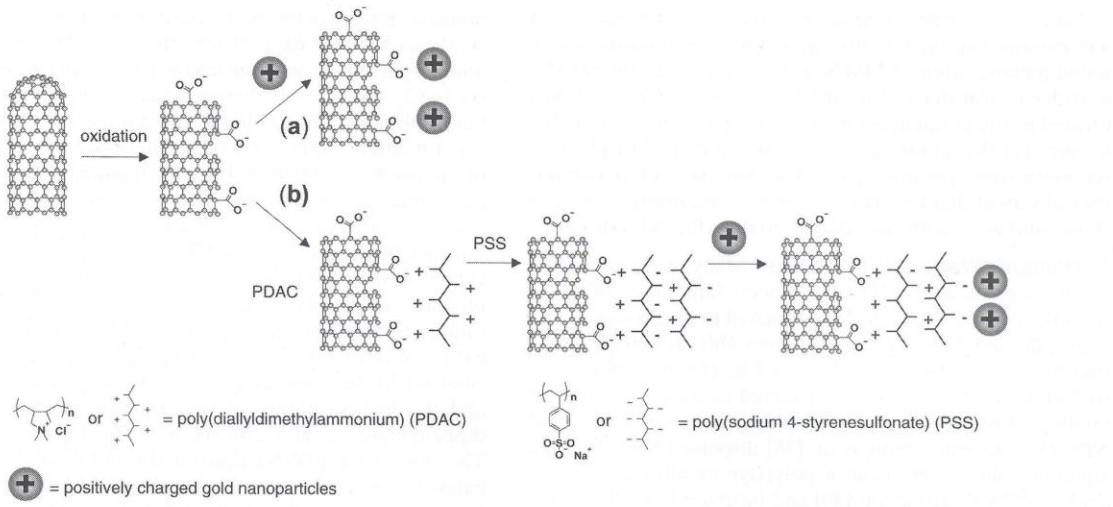

Figure 4. Decoration of oxidized carbon NTs with gold NPs by (a) direct deposition or (b) by using a bilayer of polycationic poly(diallyldimethylamm onium chloride) (PDAC) and polyanionic poly(sodium 4-styrenesulfonate) (PSS) as polyelectrolytes linkers [20].

from a direct redox reaction between metal ions and NTs. Electron transfer from SWNTs to metal ions was probed electrically, as the hole injection into SWNTs caused an increase in the electrical conductance of the SWNTs. Direct electron transfer between SWNT and metal ions depended on their relative redox potential. The Fermi level of SWNT is about +0.5 V above the redox potential of the standard hydrogen electrode (SHE) and, therefore, well above those of $AuCl_4^-$ (+1.002 V) and $PtCl_4^{2-}$ (+0.775 V), thereby explaining spontaneous electron transfer from SWNTs to the metallic anions.

Substrate-Enhanced Electroless Deposition While the above technique is an extremely simple and elegant method to decorate NTs with Au and Pt NPs, it fails for the reductive deposition of metal ions such as Cu^{2+}, Ag^+, and Ni^{2+} that have redox potentials lower than that of the NTs. This problem was solved by Qu *et al.* [32] by using a substrate-enhanced electroless deposition (SEED) technique. They were able to reduce lower redox potential metal ions to metallic NPs by using a metal substrate having a redox potential below that of the metal ions to support the NTs (Fig.6). The substrate was made by Cu to deposit Au, Pt, and Pd NPs onto NTs, while it was made by Zn to deposit Cu and Ag NPs. The metallic NP deposition was achieved *via* a galvanic cell redox reaction in which the NTs acted as a cathode for metal deposition from the reduction of metal ions in solution, while the metal substrate served as an anode on which its atoms were oxidized and retained onto the substrate. As demonstrated by the authors, this technique permitted the deposition of any metallic NP on a conducting NT as long as the redox potential of the substrate metal (Sub^{n+}–Sub^0) was lower than that of the metal ions (M^{z+}–M^0) in solution.

Water-in-Oil Nanoemulsion System A simple technique to fabricate NT-supported catalytic metal NPs that are uniformly anchored on NT sidewalls was reported by Yoon *et al.* [34]. The process was carried out at room temperature by using the water-in-oil (W/O) nanoemulsion system that the authors previously reported to fabricate Pd NPs [38]. Specifically, metal (Pd, Rh, and Pd–Rh) NPs were fabricated in a water-in-hexane nanoemulsion using

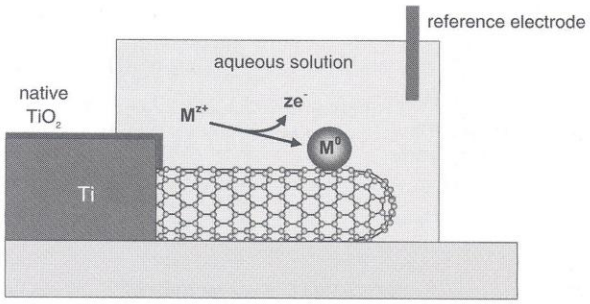

Figure 5. Electrodeposition of noble metals under direct potential control onto sidewalls of SWNTs [29].

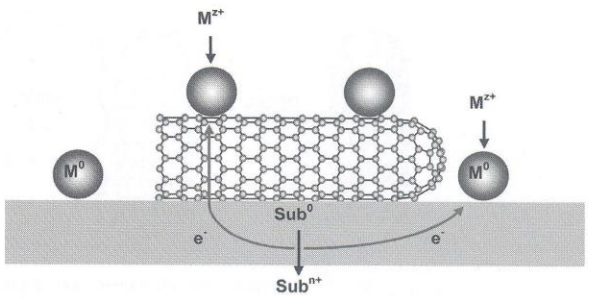

Figure 6. Electrodeposition of metal NPs onto SWNT sidewalls through substrate-enhanced electroless deposition (SEED) [32].

sodium bis(2-hexyle-thyl)sulfosuccinate as the surfactant and gaseous hydrogen (1 atm. at 25°C) as the reducing agent. Subsequently, oxidized MWNTs were added to the mixture in order to transfer to the MWNT sidewalls the metal NPs formed in the nanoemulsion. The presence and the size distribution of the NPs on NTs were studied by TEM and X-ray photoelectron spectroscopy (XPS) analyses. In particular, they observed that the NPs had lateral dimensions from 2 to 10 nm and were uniformly dispersed onto the NT sidewalls.

Surfactant-Wrapping Technique Many previous reports for linking metals to NTs have been limited to MWNTs (bundles of SWNTs) or to NTs attached to electrodes. Wang *et al.* [36] and Kamat *et al.* [37] were able to employ pNTs that had been individually dispersed by the adsorption of a surfactant on their surface that served as a template for the binding of metal ions and the subsequent growth of metal NPs. For example, Wang *et al.* [36] dispersed SWNTs in an aqueous solution by using a poly(styrene-alt-maleic anhydride) (PSMA) surfactant [39] and incubated the dispersion with Pt-(terpy)Cl_2 (terpy = 2,2′:6′,2″-terpyridine), which then electrostatically interacted with the negatively charged NTs and were reduced to form Pt NPs after addition of a $NaBH_4$ solution (Fig. 7). This technique was also used to decorate SWNTs with Pt, Au, Cu, and Fe NPs. The authors used a series of controls to confirm that the binding of metal ions to the polymeric surfactant covering the NTs was critical for controlling the growth of metal NPs. In particular, one control was in agreement with the work of Quinn *et al.* [29], whereas it did not match results reported by Choi *et al.* [31], namely, mixing PSMA-wrapped SWNTs with $Pt(terpy)^{2+}$ did not lead to a spontaneous redox reaction between the NTs to deposit platinum. The presence of NPs on the NT sidewalls was confirmed by microscopy (AFM and TEM) and (luminescence) spectroscopy. In particular, the authors observed that SWNT luminescence was partially quenched in the SWNT-Au NP assembly. Since the PSMA-wrapped SWNTs did not exhibit any luminescence quenching when simply mixed with Au NPs, the observed quenching of the assembly confirmed that gold NPs were closely attached to the NT sidewalls.

2.1.3. Applications of Metallic NPs–Decorated Carbon NTs

Catalytic Applications Many metal NPs have been used as catalysts. For instance, catalytic hydrogenation using metallic Pd particles is an important process in organic synthesis. Yoon *et al.* [34] reported that Pd NPs stabilized and dispersed by a water-in-oil (W/O) (0.04 M aqueous Na_2PdCl_4, [AOT] = 0.15 mmol (AOT = sodium di-2-ethylhexyl sulfosuccinate) in 10 ml of *n*-hexane, $[H_2O]/[n\text{-hexane}] = 15$) nanoemulsion are better catalysts for hydrogenation of olefins in an organic solvent than commercially available palladium catalysts stabilized on activated carbon. However, recycling catalytic NPs stabilized in W/O nanoemulsions is not straightforward. Use of NTs as a template for growth of catalytic NPs could solve this problem since NT–metal NP nanoassemblies could be recovered by gravitational sedimentation. The authors compared NT–Pd NP nanoassemblies, with conventional commercially available metal–carbon catalysts in the Heck coupling of iodobenzene and styrene and the hydrogenation of the coupling product *trans*-1,2-diphenylethylene at 1 atm. H_2 at 25°C (Fig. 8(a)) [34, 40]. They found that MWNT decorated with Pd NPs had a higher catalytic activity in both the coupling and hydrogenation of *trans*-1,2-diphenylethylene to 1,2-diphenylethane compared to 10 wt.% Pd on carbon. The MWNT–Pd NP nanoassemblies were much more active than the commercial Pd–C in removing benzyl ether groups (Fig. 8(b)) and reducing methyl benzoate in methanol to methyl cyclohexanecarboxylate (Fig. 8(c)). The authors also observed that the conversion of anthracene to 1,2,3,4,5,6,7,8-octahydroanthracene was higher using MWNT–palladium–rhodium NP nanoassemblies than MWNT–Pd NP or MWNT–rhodium NP nanoassemblies or a commercial Rh–C catalyst. They hypothesized that the enhanced catalytic activity of MWNTs decorated with bimetallic NPs could be owing to certain (unknown) morphologies of the palladium–rhodium nanoclusters on the NT surfaces.

Ye *et al.* [35] reported the conversion of *trans*-1,2-diphenylethylene to 1,2-diphenylethane in the presence of MWNTs decorated with Pd NPs using supercritical CO_2 as the solvent. As was observed by Yoon *et al.* [34], the MWNT-Pd NP composite exhibited a higher catalytic activity than the commercial Pd–C catalyst. Ru–Sn and Ru–Pt bimetallic Nps have been used as heterogenous catalyst [22], and gold-alkylthiol monocapped NPs [41] and Pd, Pt, Au, and Ag NPs [42] have been used as environmental catalysts.

Hydrogen Storage Kim *et al.* [43] decorated MWNTs with Ni NPs through an incipient wetness impregnation procedure [44, 45]. Ni catalyst dissociates hydrogen gas to atomic hydrogen that can chemically bond to MWNT sidewalls. The

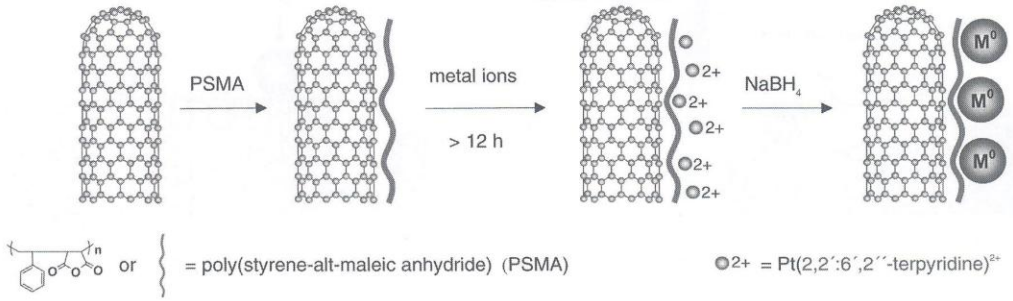

Figure 7. Solution-phase synthesis of platinum NPs–decorated SWNTs [36].

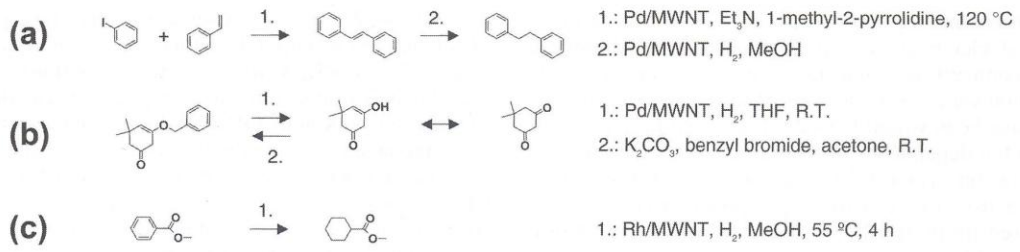

Figure 8. (a) Heck coupling of iodobenzene and styrene followed by reduction of *trans*-1,2-diphenylethylene to 1,2-diphenylethane in the presence of MWNTs decorated with palladium NPs through a water-in-oil nanoemulsion. (b) Debenzylation of 3-benzyloxy-5,5-dimethyl-3-cyclohexenone using MWNTs decorated with palladium NPs. (c) Reduction of methyl benzoate in methanol to methyl cyclohexanecarboxylate using MWNTs decorated with rhodium NPs [34].

authors reported that approximately 2.8 wt.% hydrogen was reversibly chemisorbed to MWNTs with 6 wt.% of Ni NPs, which was 0.9 wt.% higher than that of hydrogen evolved from MWNTs alone.

Fuel Cells Fuel cells are electrochemical energy conversion devices that produce electricity from a *fuel* (at the anode) and an *oxidant* (at the cathode), which react in the presence of an electrolyte. Many combinations of fuel, oxidant, and electrolytes are possible. A hydrogen cell uses hydrogen as the fuel and oxygen as the oxidant to produce energy and water as a waste. Other fuels include hydrocarbons and alcohols such as methanol and ethanol, while other oxidants include air, chlorine, and chlorine dioxide. The electrodes are usually made of metals such as nickel, carbon black, or NTs and are generally coated with a catalyst such as Pt, Pd, or Fe to improve their efficiency.

The archetypal example is the proton exchange membrane fuel cells or polymeric electrolyte membrane fuel cells (PEMFCs), in which the electrolyte also functions as a membrane between the electrodes that (1) permits the passage of the protons but not electrons, (2) prevents the transport of either H_2 or O_2 gas to the other side of the cell, and (3) is resistant to both the strong reducing and oxidizing environments at the anode and cathode, respectively. In a PEMFC several elementary steps take place at the triple-phase boundaries between the gas–electrolyte–electrode on both the anode and the cathode. For instance, at the triple-phase boundaries on the anode the following steps take place: (1) dissociative adsorption of H_2 onto the anode, (2) transfer of an electron from the H atom to the electrode to produce a proton, and (3) translocation of the proton from the electrode to the polymeric electrolyte. Therefore, both the electrodes must have a high population of the triple-phase boundary to insure efficient catalysis.

Platinum particles dispersed on carbon black (CB) electrodes have been widely used as the catalyst [46]. However, fuel cell performance is decreased because the particles trapped in the pores of CB electrodes are not involved in electrochemical reactions. Many research groups have investigated the use of NT electrodes to increase the performance of the PEMFC. For example, Matsumoto *et al.* [23] observed that a 12 wt.% Pt-deposited MWNT electrode produced a voltage 10% higher than a 29 wt.% Pt-deposited CB electrode and reduced Pt usage by 60%. The authors decorated oxMWNTs by simple reduction of a Pt salt in their presence. The higher performance of MWNT electrodes was explained by the authors by considering that (1) the Pt NPs were better dispersed on MWNTs than on the CB and therefore capable of forming more triple-phase boundaries, (2) MWNTs have high conductivity, and (3) the network of MWNTs presented spaces for gas diffusion.

Kamat *et al.* focused on the use of NTs as supporting materials in direct methanol fuel cells. In particular, they analyzed the activity of a Pt–Ru catalyst dispersed on such carbon nanostructures as SWNTs, MWNTs, carbon nanofibers, and carbon black toward methanol oxidation [26]. The authors found higher electrochemical and fuel cell performances when SWNTs were employed as the support for anchoring electrocatalytic NPs. The higher performances were explained on the basis of the intrinsic properties of SWNTs, the higher dispersion of the electrocatalyst, and the large electrochemically active surface area (ECSA). Further optimization was obtained by the authors by depositing Pt NPs onto oxidized SWNTs that were individually dispersed by use of a surfactant [37]. The polymer-wrapped SWNTs covered by Pt NPs exhibited extremely large ECSA compared to Pt–CB and Pt–MWMTs. Their Pt NPs had improved accessibility and enhanced electrocatalytic activities in reducing oxygen and oxidizing methanol. X-ray photoelectron spectroscopy of the nanoassembly indicated that the d-band center of Pt was shifted to a lower level suggesting that the electron properties of Pt had been modified to increase their ability to reduce oxygen.

Sensors Kong *et al.* [47] by using NTs decorated with Pd NPs as hydrogen sensors achieved a detection limit of 400 ppm of hydrogen. Lu *et al.* [48] used Pd NPs immobilized on SWNTs to produce a methane sensor 10 times more sensitive than conventional catalytic beads and metal oxide sensors. Kim *et al.* [49] fabricated an electrochemical sensor based on Pt NPs electrodeposited on vertically grown MWNTs to detect the concentration of in water. Qiaocui *et al.* [50] used NTs decorated with Pt NPs to fabricate a cholesterol sensor and Zhu *et al.* [51] used Pt NPs combined with Nafion-solubilized MWNTs to fabricate an electrochemical DNA sensor with enhanced sensitivity.

2.2. Semiconducting NPs

Semiconducting nanocrystals CdSe, CdS, CdTe, ZnO, ZnS, etc., which are also known as quantum dots (QDs), have

been intensely investigated because of their size-dependent optical and electrical properties [52–54]. The theoretical quantum-confined electronic states have been compared with experimental values of QDs in which diameters and shapes of QDs have been varied [55–62]. Their high luminescence yields and the dependence of their emission and absorption wavelengths on nanocrystal size and composition make QDs attractive for constructing optoelectronic devices with tailored properties [63, 64] and for *in vivo* biosensor applications [65].

NTs have promise for use as intracellular delivery systems and nanoprobes. Unlabeled SWNT can in principle be visualized by their infrared photoluminescence [66, 67] after excitation in the near-infrared. The ability of near-infrared light to penetrate tissue and the reduced auto-luminescent background in tissue and blood allow their use for biomedical applications [68, 69]. However, the photoluminescence intensity of SWNTs is too low to be visualized using optical microscopy. In contrast, common luminophores such as organic dyes and QDs have relatively high quantum yields that are approximately 1000 times higher than that of SWNTs [70, 71]. QDs have quantum yields at room temperature that are similar to those of frequently used organic dyes such as rhodamine 6G, fluorescein, and Texas Red, but have larger absorption cross sections and lower photobleaching rates. Bawendi *et al.* [72, 73] calculated that the molar extinction coefficients of CdSe QDs were approximately 10–100 times larger than those of organic dyes. While Chan *et al.* [65] calculated that ZnS-capped CdSe QDs were approximately 20 times brighter and approximately 200 times more stable than rhodamine 6G molecules. Therefore, QDs are excellent candidates for generating luminescent nanoprobes and hybrid nanoassemblies. The decoration of NTs with QDs would afford nanoassemblies that are visible by optical microscopy. In addition the high aspect ratio of NTs would permit multiple functionalization(s).

Generally, QDs have been linked to oxidized and pristine NTs through covalent and noncovalent chemistries, respectively. *In situ* growth of QDs on NTs is another method for preparing QD–NT conjugates. The choice of the chemistry and the linkers between the NTs and the QDs has typically been dictated by the application of the nanoassembly, namely, (1) electron donor–acceptor arrays for use in photovoltaics, and (2) luminescent nanoassemblies for use in nanophotonics and quantum computing, and as biomedical research probes. Because this chapter focuses on NT-based macromolecular nanoassemblies, the decoration of oxidized NTs using covalent chemistry is not discussed. Interested readers can find examples in Refs. [74–77].

Functionalization of oxNTs is usually based on derivatization of the carboxylic groups produced by oxidation in strong acid [18], which attacks not only the NT ends but also a remarkable percentage of the sidewalls. This observation is consistent with Raman studies which show that the D-band Raman intensity (the measure of sp^2 disorder in an NT) increases significantly upon acid purification of NTs [78–81]. As observed by Haremza *et al.* [76] sidewall (covalent) functionalization disrupts the π-bonding symmetry of the sp^2 hybridization of the NTs to compromise their unique properties necessary for electronic devices. Sidewall oxidation is acceptable for applications such as biosensing and for realizing composites in which the electronic properties of NTs are not essential. For donor–acceptor systems intact electronic properties are extremely important. Thus, the use of oxNTs is unsuitable for this purpose. The decoration of oxidized NTs with QDs produces nonuniform surface coverage as the semiconducting nanocrystals are linked to the oxidized NTs at their open ends and sidewall defects where carboxylic groups introduced by oxidation are localized. In contrast, noncovalent chemistry, which permits the generation of NT-based supramolecular nanoassemblies with higher control of many properties in the final structure, are more suitable for the fabrication of both photovoltaic devices and luminescent nanoprobes because their electronic properties can be preserved and a more uniform surface coverage can be obtained. Furthermore, by choosing the kind of tether and chemistry to link the QDs to the NTs many type of properties, including the electronic contact and the strength of the attachment between QDs and NTs, can be finely tuned. The choice of a specific tether can change another important property of the final adduct, namely its cytotoxicity [82]. Nanoassemblies based on QDs and NTs could be extremely useful in biomedical research owing to the excellent optical properties of QDs and the high aspect ratio of NTs. However, before developing *in vivo* or *in vivo* application(s) the cytotoxic effects of NTs and QDs must be carefully evaluated. Many recently introduced NPs such as NTs [83–86], fullerenes [87], QDs [88], and GNPs [89] have shown signs of toxicity that were dependent upon such factors as dose, dimension, chemical functionalization, and physical aspect (morphology). The use of a specific tether could profoundly change the cytotoxicity profile of the QD–NT nanoassembly and, therefore, permit its applicability to biomedical research, for instance, to fabricate intracellular drug and/or gene delivery systems.

In the following pages, we discuss the macromolecular decoration of NTs with QDs through noncovalent chemistries such as polymer wrapping [91, 92, 94], enzymatic-driven biotinylation [95], addition chemistry [100], macromolecular adsorption [107], and π–π interactions with aromatic molecules [109, 110]. In the subsequent section we will discuss the *in situ* growth of QDs on NT sidewalls.

Polymer Wrapping The prevention of the fluorescence quenching of QDs on NTs by a polymeric linker would permit visualization of NTs by routine fluorescent microscopy and their use as photoluminescent probes. Sodium dodecyl sulfate (SDS) was reported to individually disperse NTs in an aqueous environment through interaction of its hydrophobic dodecyl tail with the carbonaceous NT sidewall accompanied by the exposure of the hydrophilic sulfate head to the environment [66, 90]. Chaudhary *et al.* [91] reported that small bundles of SDS-wrapped SWNTs were visualized by decoration with ZnS-covered CdSe QDs in which the Zn^{2+} ions were coordinated with the sulfonate oxygens on the dispersed NT sidewalls (Fig. 9). The nanoassembly could be visualized by routine fluorescence microscopy because the SDS layer prevented fluorescence quenching caused by charge injection from the excited states of the QD into the conduction band of the SWNT, which functioned as a quencher. Although this study showed that this nanoassembly was luminescent, it was not applicable for biomedical research since the 1% SDS concentration used was toxic to many biological systems.

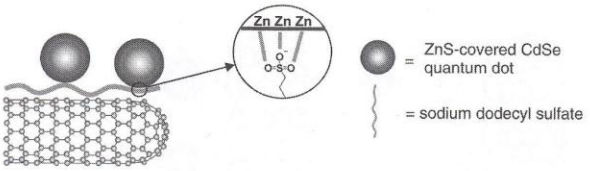

Figure 9. Decoration of pristine SWNTs with ZnS-encapsulated CdSe quantum dots through the coordination of zinc ions to oxygen atoms in the sulfonate groups of the surfactant wrapping the NTs [91].

Olek *et al.* [92] reported a novel strategy for the fabrication of NT–QD nanoassemblies. MWNTs were prefunctionalized without introduction of sidewall defects by nondestructive wrapping with a polymer (poly(allylamine hydrochloride) or SiO_2). QDs were then covalently linked to the amine groups protruding from the polymer surface by ligand exchange chemistry. By choosing the type of polymer the authors were able to control the contacts between electron donors (QD) and electron acceptors (MWNT), thereby allowing or preventing the quenching of fluorescence owing to charge transfer or tunneling from photoexcited QDs to MWNTs. In particular, poly(allylamine hydrochloride)-coated MWNTs could quench the fluorescence of their linked QDs, while MWNTs coated by a thick and uniform layer of SiO_2 could not quench QD fluorescence. The authors postulated that the large band gap and thickness of the silica layer prevented quenching by both charge transfer and electron tunneling.

Our research group obtained a result similar to that described by Olek *et al.* [92]. In our case the surface of SWNTs was silylated by ultrasonication in the presence of a thiolated organosilane, and subsequently the functionalized SWNTs were isolated by ultracentrifugation [93, 94]. The collected supernatant fraction was demonstrated to contain small bundles of SWNTs that were coated by a thin layer of the organosilane, which had adsorbed onto the NT sidewalls through the thiol group, leaving the trimethoxy- (or trihydroxy-) silyl group protruding from the adduct surface (Fig. 10(I)). A second layer of the organosilane was then deposited onto the silylated surface so that amino or thiol groups were exposed (Fig. 10(II)) for linkage to QDs (Fig. 10(III)). Photoluminecence characterization of the final adduct suggested that the thin layer of silica between QDs and SWNTs was able to prevent the quenching of luminescence by SWNTs. The silylation of NT sidewalls will be described in more detail later in this chapter.

Biochemical Approach Didenko *et al.* [95] reported an enzyme-driven technique for labeling SWNTs with QDs. The biotinylation of SDS-stabilized SWNTs was obtained by the application of the reaction between tyramide and horseradish peroxidase (HRP) [96]. HRP converts biotinyl tyramide to the active biotinyl tyramide radical that reacts with NT sidewalls to give biotinylated SWNTs. The functionalized SWNTs were then treated with streptavidin (Str)-conjugated QDs (Fig. 11) or Str-conjugated FITC. Verification of an NT labeling was obtained by TEM. Because the QD-SWNTs were visible by simple optical microscopy, the fluorescence quenching by SWNTs was avoided. Unfortunately, the photoluminescence of FITC was quenched.

The FITC quenching was caused by energy transfer between the fluorophore (donor) and the NT (acceptor) and has been shown for a variety of luminescent molecules such as Alexa Fluor-488, 3,3′-dipentyloxacarbocyanine iodide, pyrene [97], and naphthalimide chromophore [98]. Luminescence quenching was observed for fluorophores both covalently and noncovalently linked to NTs. However, noncovalent attachment of a luminophore to an NT sidewall through a linker could result in incomplete energy transfer from the photoexcited luminophore to the ground-state acceptor (NT) if the spacer prevented the complete contact between the luminophore and the NT sidewall. If the spacer is long enough, luminescence can be maintained as was shown in the case of FITC positioned at the end of a 25-mer oligonucleotide, which was subsequently hybridized to a complementary DNA strand attached to the SWNT [99]. In the latter case, the distance between the FITC and the NT prevented any energy transfer.

Didenko *et al.* linked FITC and QDs to SWNTs using the same tyramide linker but only the FITC was quenched. The authors considered that the quenching interactions between the QD core and NT surface were limited by (1) QDs being bigger than the NT diameter, and (2) their coating by a protective polymeric shell and Str.

Addition Chemistry Similarly to the technique reported by Didenko *et al.* [95], Biju *et al.* [100] reported the decoration of

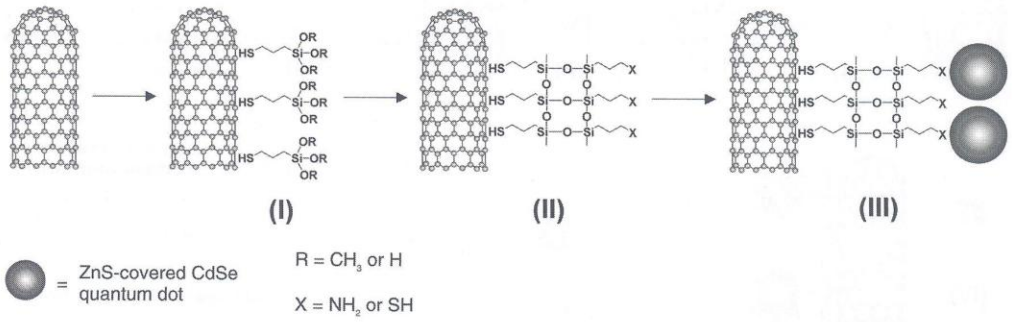

Figure 10. Decoration of SWNTs with quantum dots by stepwise silylation of NT sidewalls. (I) SWNTs were first silylated through adsorption of a thiolated organosilane. (II) Condensation of a second layer of organosilane modified the surface of coated SWNTs with amino or thiol groups (III) to which quantum dots were linked [94].

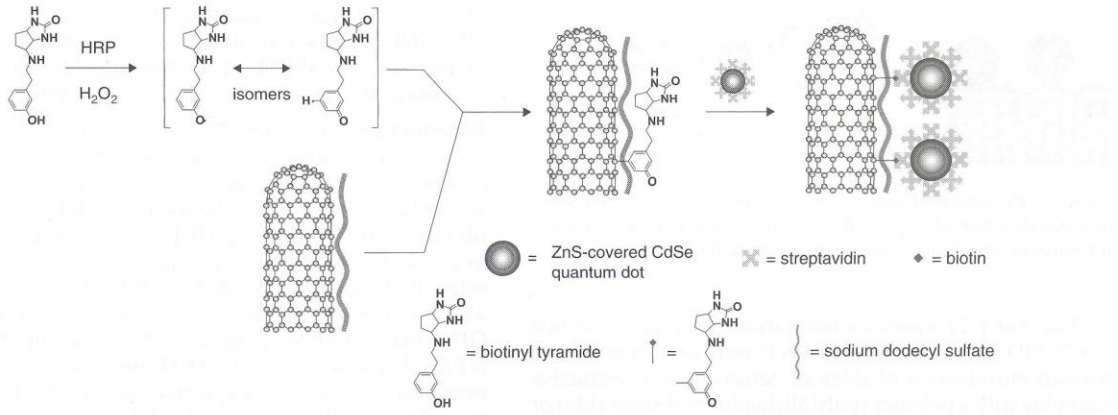

Figure 11. Biotinylation of SWNTs by biotinyl tyramide radicals generated by HRP and subsequent decoration with Str-conjugated ZnS-covered CdSe quantum dots [95].

biotinylated SWNTs with Str-conjugated ZnS-covered CdSe nanocrystals. They also analyzed the effect of conjugation of QDs to SWNTs on QD photoluminescence. The authors used a multistep procedure to prepare QD-decorated SWNTs (Fig. 12). They first functionalized SDS-coated NT sidewalls by treatment with an aromatic diazonium salt followed by reduction as reported by Dyke and Tour [101, 102] to obtain biotinylated SWNTs. Specifically, surfactant-stabilized SWNTs were allowed to react with *p*-nitrophenyldiazonium tetrafluoroborate (NDTF) in water at 10°C for 96 h (step I). The surfactant SDS has been reported to produce stable suspensions of individual SWNTs [66]. Dyke and Tour hypothesized that the diazonium salt could migrate through the layer of surfactant to the NT sidewall surface, where an electron was transferred from SWNT to the diazo moiety to form a reactive aryl radical that reacted with the graphitic wall of the NTs. Subsequently, the *p*-nitrophenyl groups on the SWNT surface were reduced to *p*-aniline groups using $NaBH_4$ in dry DMSO (step II). The *p*-aniline moieties were reacted with biotin-*N*-hydroxysuccinimide ester (BHSE) to functionalize the NT sidewalls with acylated biotin groups (step III), which then bound the Str decorating the QDs (step IV).

By means of atomic force microscope (AFM) and field emission scanning electron micrographs (FESEMs) the authors confirmed the decoration of SWNTs with semiconducting nanocrystals and, more importantly, that the loading of QDs on the NT sidewalls can be decreased (or increased) by simply decreasing (or increasing) the concentration of the QD solution mixed with the biotinylated SWNTs (step IV). The authors observed that the photoluminescence of QD–SWNT adducts in distilled water was quenched by approximately 30% with respect to free QDs and that the QD–SWNT conjugates exhibited reduced photoluminescence lifetimes compared to those of nonconjugated QDs. The authors attributed the quenching of the photoluminescence intensity and

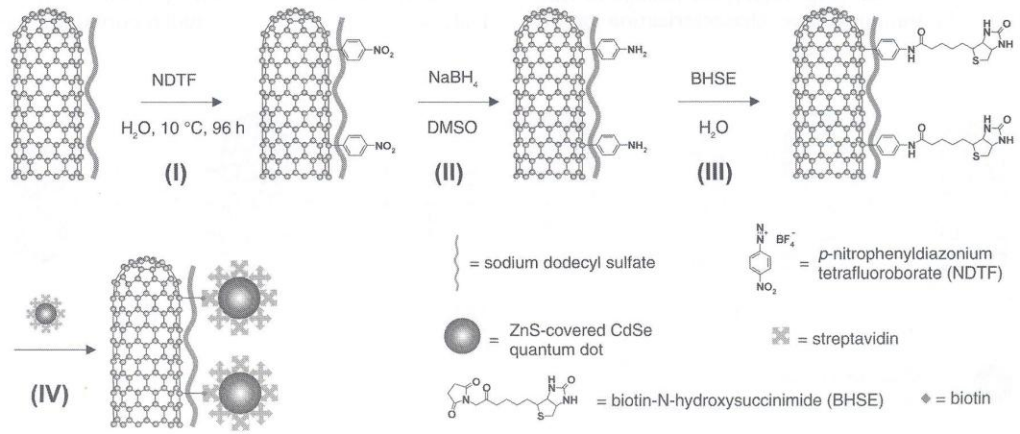

Figure 12. Biotinylation of SWNTs by addition reaction of an aromatic diazonium salt, reduction, biotinylation, and subsequent decoration with Str-conjugated ZnS-covered CdSe quantum dots [100].

lifetime to fluorescence resonance energy transfer (FRET) from the semiconducting nanocrystals to the NTs. Generally speaking FRET involves nonradiative energy transfer between a donor (in its excited state) and an acceptor (in its ground state) if three requirements are met: (1) overlap between the absorbance spectrum of the acceptor and the emission spectrum of the donor; (2) coupling between donor and acceptor transition dipoles; and (3) spatial proximity of donor and acceptor (distance less than 10 nm). However, the FRET efficiencies calculated from the value of the photoluminescence intensity and that of lifetime luminescence exhibited discrepancies. Therefore, the authors concluded that the observed photoluminescence quenching was caused by not only FRET between QDs and SWNTs but also by other factors such as electron transfer (from QDs to SWNTs) and destabilization of QD excitons.

Macromolecular Adsorption Functionalization of both SWNTs and MWNTs with macromolecules has gained increasing interest because of their potential use in supramolecular nanoassemblies for biosensors and intracellular protein transporters.

Str, which is a 64 kDa tetrameric protein having a 5 nm diameter, has potential applications in anticancer therapy and diagnostics [103]. Str adsorbs onto the sidewalls of pristine MWNTs [104, 105] and oxidized SWNTs [106]. Our research group decorated SWNTs with Str-conjugated ZnS-encased CdSe QDs (Fig. 13) [107, 108]. The resulting SWNT–Str-QD nanoassembly fully dispersed in physiologic buffer and was visible by conventional luminescent microscopy. In steady-state experiments, SWNT–Str-QD in PBS exhibited an emission band that was only slightly quenched (<10%) and blue shifted with respect to free SA-QD in PBS.

Thus, our results did not fully agree with the photoluminescence properties of the QD–SWNT adduct reported by Biju *et al.* [100]. These authors reported a quenching of the QD–SWNT photoluminescence (compared to that of free Str-QDs) higher than that observed by our group and did not observe any shift in the emission profile of QD–SWNTs compared to that of free Str-QDs. These differences could be explained by the fact that Biju *et al.* had biotilnylated the NT sidewalls by an addition reaction that was able to (1) exfoliate and enrich the solution of individual NTs, and (2) profoundly modify the spectroscopic properties of SWNTs [101, 102]. We used pristine SWNTs that were initially clumped together and subsequently dispersed in PBS through the adsorption of Str coating the QDs and, as revealed by TEM, the process was not able to totally exfoliate the SWNTs, and small bundles of NTs were still present. Differences in the aggregation state and the spectroscopic properties of the NTs could, therefore, explain the differences in the photoluminescence properties of the final QD–SWNT adducts.

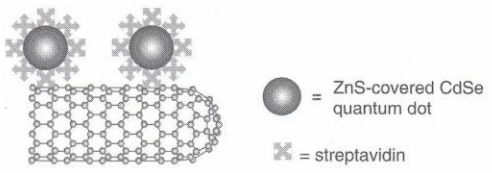

Figure 13. Decoration of pristine SWNTs with quantum dots using Str as a linker [107].

Three reports had been published [95, 100, 107] regarding the decoration of SWNTs with Str-conjugated ZnS-covered CdSe QDs to form a luminescent SWNT-based nanoassembly that was (1) visible by conventional luminescent microscopy, (2) dispersible under physiologic conditions, and (3) further functionalizable with biotinylated macromolecules using the Str molecules extruding out of the adduct and the strong affinity between biotin and Str ($K_D = 10^{-15}$ M). Our research group investigated the ability of SWNT–Str-QD to function as a multivalent intracellular fluorescent nanoprobe in Jurkat T leukemia cells to which biotinylated mouse antihuman CD3 antibody bound to surface CD3 receptors. The nanoassembly was readily internalized by Jurkat T cells suggesting that the binding of the nanoassembly to CD3 was able to induce signaling through the T cell receptor (TCR), and that signaling-induced endocytosis led to internalization of the antibody-conjugated nanoassembly. TCR signaling induced by crosslinked antihuman CD3 with or without antihuman CD28 is followed by receptor internalization, which is a mechanism of signaling down regulation (post-TCR-signaling endocytosis). After internalization nanoassemblies were transported into lysosomal compartments (Fig. 14) [108]. Therefore, the SWNT–Str-QDs represent a potentially excellent scaffold for constructing intracellular multivalent nanoprobes.

π–π Interactions with Aromatic Molecules While using particular polymers to link SWNTs and QDs would avoid energy transfer and permit the use of fluorescent NTs for sensorial and biomedical applications, use of aromatic molecules as linkers would facilitate energy transfer for photoactive material applications. Guldi *et al.* [109] nondestructively decorated SWNT sidewalls with 1-(trimethylammonium acetyl) pyrene (pyrene$^+$) that were adsorbed through π–π interactions. The positively charged trimethylammonium group allowed the SWNTs to associate with negatively charged thioglycolate-stabilized size-quantized CdTe QDs (namely, red- and green-emitting nanocrystals, having lateral dimensions of 5 and 2.4 nm, respectively) to produce a photoactive supramolecular nanostructure (Fig. 15). The strong electronic interactions in the ground and excited states of this nanoassembly were responsible for the favorable charge transfer between its components and allowed Guldi *et al.* to prepare a novel hybrid cell by sequential layering that, in response to visible light irradiation, performed as a photoelectrochemical device.

A similar noncovalent method for making CdSe-decorated SWNTs that was based on the π–π interactions between SWNTs and aromatic molecules was reported by Li *et al.* [110]. In this case trioctylphosphine oxide (TOPO) cover on the QDs was displaced by pyridine molecules. Because CdSe QDs display good electron affinity and pyridine is a good electron donor, owing to the isolated electron pairs on nitrogen, the coordination between the QDs and pyridine molecules is stable. Ligand exchange increased the QD–SWNT affinity, probably through conjugated NT-pyridine π–π interactions, and permitted the nonchemical decoration of SWNTs with discrete

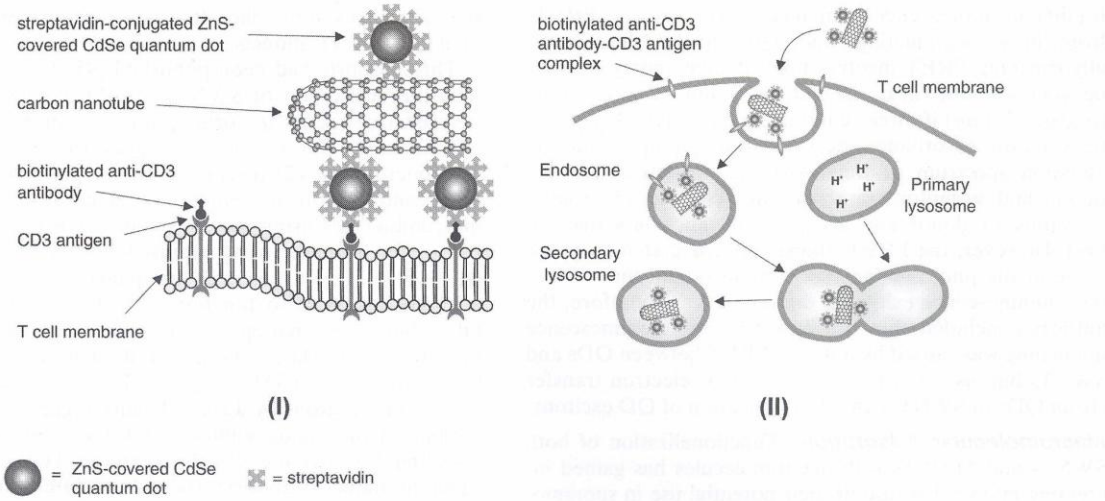

Figure 14. (I) A biotinylated anti-CD3 monoclonal antibody was used to link CD3 to the nanoassembly. The supramolecular luminescent nanoassembly acted as a multivalent delivery system, with each nanoassembly capable of binding many biotinylated anti-CD3–CD3 receptor complexes. (II) The nanoassemblies were delivered into T cells through post-TCR-signaling endocytosis and transported into secondary lysosomes through the fusion of endocytotic vescicles with primary lysosomes [108].

pyridine-covered QDs or a uniform layer, depending on the QD–SWNT ratio and reaction time. Raman spectroscopy, which indicated photoluminescence quenching of the QDs owing to their interaction with the SWNTs, suggested that energy transfer occurred from the CdSe donor to the SWNT acceptor.

2.2.1. *In Situ* Growth

In the above section, we described the noncovalent decoration of NTs with chalcogenide (sulfides, selenides, and tellurides) NPs. The reported processes generally required multiple steps with variable yields and necessitated intermediary linkers. Both pristine and oxidized NTs have also been used as templates for direct thermal growth of CdSe [111, 112], ZnO [113] and ZnS [114] QDs or *in situ* wet chemical synthesis of CdS [115–116], ZnS [118], SnO_2 [119], and TiO_2 [120] QDs. Independent from these reported techniques, others observed that introducing functional groups on the NT surface benefited QD growth. For example, Banerjee *et al.* reported the *in situ* thermal growth of CdSe and CdTe QDs onto the sidewalls of heavily oxidized SWNTs [111] and MWNTs [112]. This technique involved metal cation coordination to the oxygenated functional groups on the surface NTs to form specific nucleation sites for the QD growth. Oxidation opened and derivatized most of the NT ends as well as attacked occasional sidewall defect sites to probably carboxylic acids, alcohols, and ketones. The degree of QD immobilization correlated with the extent of NT oxidation. Only aggressive oxidation enabled high surface coverage by the QDs on the open ends and serrated edges of the NTs. Few, if any, QDs were observed coordinated with pristine or weakly oxidized NTs. Crystal growth had predominantly the mineral form of zinc sulfide, though at least some crystals appeared to have the cubic morphology of zinc blend. The *in situ*–generated QDs varied widely in shape and size. The anisotropic QD formation could be caused by the NT bulk, which would spatially hinder access to one side of the growing crystallites, thereby causing variations in crystal lattice. The role of the NT on the shape and dimension of the QD depended on such factors as functional group density at particular sites, site geometry, and functional group separation on the same or adjacent tube.

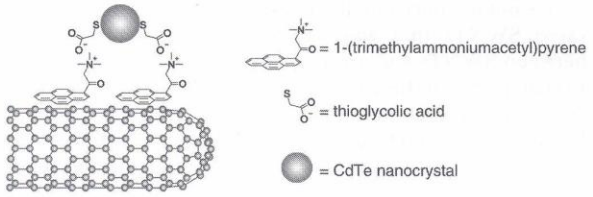

Figure 15. Decoration of pristine SWNTs using a bifunctional linker [1-(trimethylammonium acetyl) pyrene] adsorbed onto NT sidewalls through *via* π–π interactions and electrostatically linked to thioglycolate-stabilized quantum dots [109].

2.3. Insulating NPs

Silica nanoparticles (SNPs) have been widely used for biosensing and catalytic applications owing to their large surface area-to-volume ratio, straightforward manufacture and the compatibility of silica chemistry to covalent coupling of biomolecules. The physical (diameter and porosity) and chemical properties of SNPs doped with fluorescent, magnetic, or biological macromolecules can be easily tuned. Therefore, NT–SNP nanoassemblies could be an excellent scaffold on which higher-order structures can be constructed.

Polymeric NPs can be prepared by several methods, including the widely used Stobër technique [121] and the water-in-oil (W–O) nanoemulsion system [122]. The former is based on hydrolysis of a silica precursor in an alcoholic medium containing ammonia. The latter uses water droplets inside of reverse micelles as nanoreactors to regulate the size of the final NPs, which is based on the water droplet dimension and, therefore, by the molar ratio of water-to-surfactant and precursor. Other parameters relevant to final NP size are molar ratio of precursor to catalyst, precursor reactivity, and reaction time and temperature.

Our research group explored several techniques to achieve nanoassemblies between SNPs and NTs (Fig. 16) [123–125]. As illustrated in Figure 15, silylation of pNTs and oxNTs employed a silica precursor adsorbed onto pNTs through a pyrenyl group [*N*-(3-trialkoxy)propyl) 3-(pyrenyl)propionamide] and coupled to oxNTs through a carboxamide bond [*N*-(3-trialkoxypropyl) acetamide], respectively. SNPs were also prepared separately and then coupled to NTs (method I) or grown directly on NTs in a W–O nanoemulsion (method II). The resulting nanoassemblies had the following properties:

1. SNP loading depended on silylation level of NT sidewalls.
2. SNP decoration occurred only at NT sites that were functionalized with silane, whereas the bare graphitic NT sidewall did not associate with SNPs.
3. Both the methods decorated NTs with individual SNPs. However, only the second method produced uniform silica coating on the NTs.

Nondestructive functionalization of the pNT sidewalls was conducted by the π–π adsorption of a pyrenyl-terminated silica precursor onto the pNTs. The level of silylation of pNTs was tuned by the weight ratio between the silica precursor and the NTs. Silylation of oxNTs was conducted by coupling an amino-terminated silica precursor (3-aminopropyltrimethoxysilane or 3-aminopropyltriethoxysilane) to the carboxylic acid groups of the oxNTs. Thus, the level of silylation of oxNTs depended on their oxidation level. Then, mild oxidation introduces carboxylic groups only at the NT tips so that nanoassemblies were comprised of NTs having SNPs only at these position ends. Such a result could not be achieved by simple adsorption onto pNTs, which could not be spatially controlled.

In method I, previously grown SNPs were linked to silylated NTs. The resulting nanoassemblies were composed of full-length or shortened NTs decorated with SNPs. In method II, the SNPs were grown directly on the silane groups protruding from the NT sidewalls by means of a water-in-oil nanoemulsion system. SNPs that had a diameter smaller than that of the NTs grew individually on the NT sidewalls, whereas those with a larger diameter could uniformly coat the NTs if the level of silylation was high. Small reverse micelles, having approximately the same diameter as the NTs, were not able to totally embed the NTs and, therefore, could only nucleate the growth of the SNPs on the NT surface. Large reverse micelles that could fully embed the NTs were able to nucleate growth of the SNPs around the NTs. At high silylation levels, the micelles were close enough together to fuse and totally embed the NTs so that a uniform layer of silica grew around the NTs.

Our group fabricated nanoassemblies composed of full-length and oxidized NTs linked to SNPs doped with a ruthenium complex fluorophore (tris(2,2′-bipyridyl)ruthenium(II) chloride hexahydrate) using method I [125]. We observed that the fluorophore remained fluorescent after encapsulation into

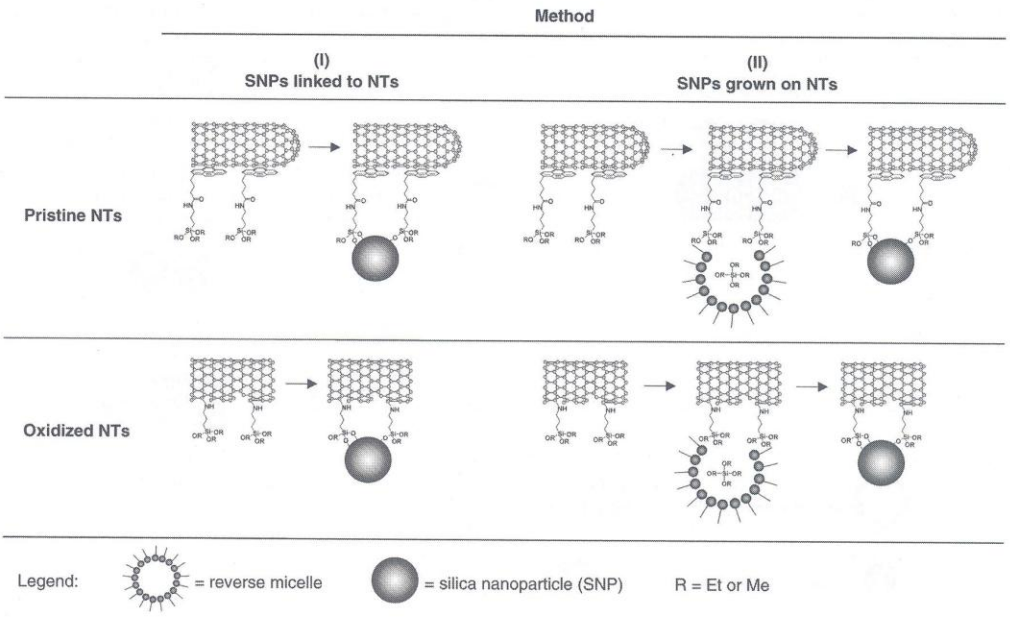

Figure 16. Functionalization of both pristine and oxidized carbon NTs with silica nanoparticles (SNPs) [123–125].

the SNPs and their attachment to the NT sidewalls. Therefore, the silica host was able to avoid fluorescence quenching caused by charge injection from metal-to-ligand charge transfer excited states of the fluorophore into the conduction band of the NT quencher. These fluorescent nanostructures, particularly one containing full-length pNTs, which have an intact π-electron structure, may be useful for applications ranging from biosensors to electronics.

Nondestructive silylation of NTs using organosilanes terminated by functional groups that adsorb onto the NT sidewalls has attracted recent interest for the possibility of combining the properties of pristine NTs and sol–gel material chemistry. Liu *et al.* [126] showed that SWNTs dispersed in dimethylformamide adsorbed onto a NH_2-functionalized silica surface but not on a CH_3-functionalized surface. Fu *et al.* [127] reported the silylation of SWNTs through the adsorption of an amino-terminated organosilane dispersed in ethanol because SWNTs have metallic or semiconducting behavior (depending on their chirality) and silica acts as a perfect insulating material. Thus, individually dispersed full-length (pristine) SWNTs coated by a uniform silica layer represent an excellent building block for nanoelectronic devices. Our research group investigated the dispersion of SWNTs in pure water by ultrasonication in the presence of a thiolated organosilane, mercaptopropyl trimethoxysilane (mptmos). We observed that after ultrasonication and subsequent ultracentrifugation the collected supernatant fraction mainly contained individual–small bundles of SWNTs coated by a thin uniform layer of organosilane (Fig. 17(a)). Recently, Zanella *et al.* [128] reported the deposition of GNPs onto MWNTs functionalized with aliphatic bifunctional thiols. This group hypothesized that the thiols reacted with the defective pentagonal sites on the sidewalls of the NTs. We hypothesized and then demonstrated that the thiol groups of mptmos adsorbed onto the SWNT sidewalls leaving the trimethoxy- (or trihydroxy- posthydrolysis) silane group protruding from the NTs (Fig. 17(a)) [93].

Ultrasonication of an aqueous dispersion of SWNTs in the presence of mptmos and subsequent ultracentrifugation gave a clear and slightly colored supernatant that was stable in water and did not show sedimentation after several months. The absorbance spectrum of the supernatant exhibited sharp peaks in the visible range corresponding to electronic transitions between the van Hove singularities of metallic and semiconducting NTs to suggest that the supernatant was composed by individually dispersed NTs. Generally speaking, the quasi one-dimensionality of an NT causes its density of states to be characterized by a series of singularities located at energies depending upon the reciprocal NT diameter. Therefore, the absorption spectrum of an NT is expected to be composed of a series of sharp peaks corresponding to the transitions between the van Hove

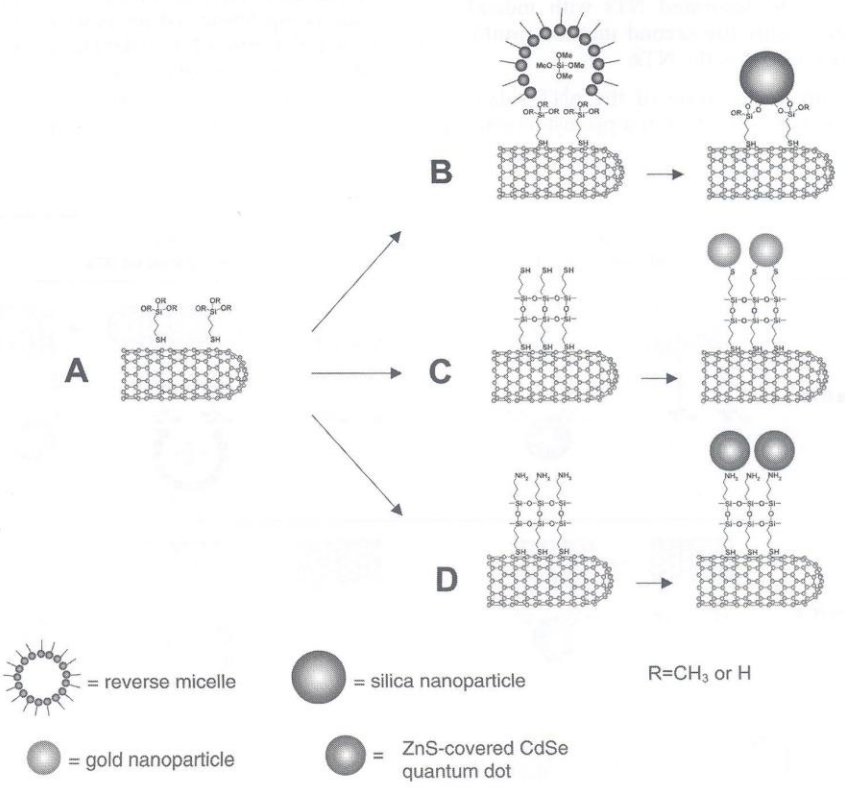

Figure 17. Dispersion of pristine SWNTs by a thiolated organosilane to provide supramolecular nanoassemblies [93, 94].

singularities. Since NTs grow with different chiralities, the absorption spectrum of a batch of NT is expected to be the superposition of distinct electronic transitions, each arising from a specific chirality. Well-defined electronic transitions are indicative of weak interactions between NT through side-to-side van der Walls contact. Therefore, the intensity and shape of the electronic transitions in the absorption spectrum give an indication of the level of aggregation of the NT. TEM images of the dispersion showed the presence of fiber-like material less than 10 nm in diameter and 500–1500 nm long. These results confirmed that the supernatant fraction, collected after mptmos-assisted ultrasonication and subsequent ultracentrifugation, was composed of small bundles of pristine SWNTs coated with a uniform layer of mptmos molecules that were stably dispersed in water.

The exposed functional groups on NTs can offer flexible ways for preparing NT-based supramolecular nanoassemblies by sol–gel chemistry. We reported the decoration of silylated SWNT with SNPs (Fig. 17(b)) and GNPs (Fig. 17(c)), and thereby demonstrated a method by which an organosilane could be adsorbed onto SWNT and the excellent versatility of the final adduct. By a three-step process, we decorated silylated NTs with QDs to investigate the electronic properties of the adsorbed silica thin layer (Figs. 10 and 17(d)) [94].

2.4. Magnetic NPs

NT-magnetic (m) NP nanoassemblies have tremendous potential applications for magnetic materials, functional nanomaterials, and nanodevices owing to their general and facile fabrication.

Correa-Duarte *et al.* [129] reported a procedure to load Fe_3O_4–γ-Fe_2O_3 NPs onto the surface of MWNTs by combining polymer wrapping and layer-by-layer self-assembly techniques (Fig. 18). First, a negatively charged polyelectrolyte [poly(sodium 4-styrenesulfonate), PSS] was used as a wrapping polymer to provide a stable aqueous dispersion of negatively charged NTs. Because of the high density of sulfonate groups, PSS acted as a primer on the NT sidewalls for the subsequent electrostatic adsorption of the cationic polyelectrolyte poly(diallyldimethylammonium chloride) (PDAC). The latter ensured the efficient adsorption of negatively charged mNPs onto the NT sidewalls through ionic interactions. TEM images showed that NTs were completely covered with a dense layer of mNPs.

The reported technique permitted alignment of NTs under relatively low magnetic fields. After a drop of NT–mNP dispersion was dried onto a Si wafer in the absence of an external field, the NT–mNPs were found randomly oriented on the silicon substrate. However, NT-mNP could be oriented in the plane of a silicon wafer by applying an external magnetic field parallel to the substrate. The NT–mNP became aligned as long-chain structures on a silicon substrate at 300 K, since magnetic NTs suspended in a liquid align parallel to the direction of the applied magnetic field. The authors found that the volume magnetization of NT–mNP was enhanced by 17% compared to the pure powdered mNPs. This result suggested that either the process of adsorption onto NT sidewalls changed the particle magnetization or the NTs carry an intrinsic magnetization caused by the catalyst (usually Ni) used for the growth process.

Georgakilas *et al.* [130] described a strategy to functionalize SWNTs with preformed mNPs (oleic acid–capped iron oxide, cobalt, and cobalt–platinum NPs) through a carboxylic acid derivative of pyrene (CDP) (obtained from Schiff condensation of the commercially available pyrenecarboxyaldehyde with aminoundecanoic acid) (Fig. 19). The procedure relied on the ability of pyrene to adsorb onto the NT surface through π–π stacking interactions. The carboxylic groups of the pyrene derivative were then linked to metal or metal oxide NPs by stirring the mixture without heating or sonication. Linkage was signaled by a change in the color of the solution to dark brown and the gradual solubilization of the NTs. The inorganic nanoclusters were well dispersed on the SWNT surface. The capped mNPs were highly soluble in organic solvents, such as chloroform, toluene, and hexane.

Gao *et al.* [131] explored a facile, general, and effective approach of loading NTs with mNPs that overcame some shortcomings of the approach reported by Georgakilas *et al.*

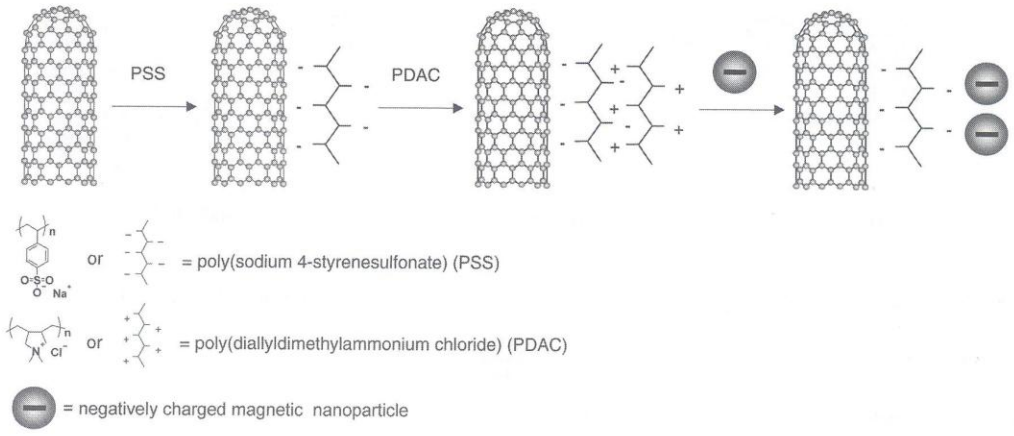

Figure 18. Decoration of MWNTs with magnetic NPs through polymer wrapping and layer-by-layer self-assembly [129].

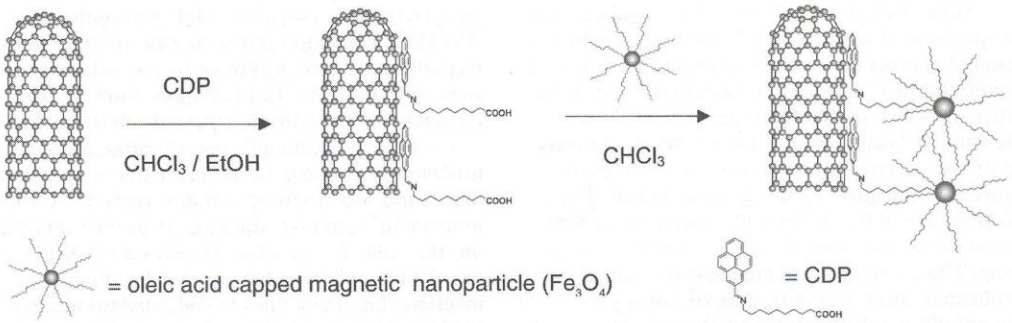

Figure 19. Decoration of carboxylated SWNTs with capped magnetic NPs [130].

[130]. Specifically, according to Gao *et al.*, the disadvantages of the Georgakilas *et al.* method are (1) the attachment of mNPs to NTs is very weak because the attaching force of π–π stacking interaction is not strong and could be weakened by the weight of iron oxide particles in the mNPs; (2) the loading capacity by the mNPs is quite low because of the weak linkage, which limits the applications of the product; and (3) the attaching process would be even less effective on MWNTs because the surface area per gram of MWNTs is much smaller. The authors reported a general approach to supramolecular magnetic nanotubes (mMWNTs) that overcame these shortcomings based on (1) covalent grafting of cationic polymer chains onto MWNT surfaces and (2) assembling mNPs onto the polyelectrolyte-coated MWNTs. The specific synthetic procedures are depicted in Figure 20. First, the oxMWNTs were allowed to react with excess thionyl chloride and ethylene glycol to generate 2-hydroxyethyl-functionalized MWNTs (hMWNTs), which were treated with 2-bromo-2-methylpropionyl bromide (BMB) to provide the MWNT-based macroinitiator (MWNT-Br) [132]. Next, poly(2-diethylaminoethyl methacrylate) was covalently grafted onto MWNTs by *in situ* atom-transfer radical polymerization of 2-diethylaminoethyl methacrylate (DEAEMA), which was initiated with MWNT-Br in presence of CuBr and *N*,*N*,*N*′,*N*″,*N*‴-pentmethyl-diethylenetriamine (PMDETA). Then, the polyamine-grafted MWNTs (MWNT-*g*-PAm) were quaternized with methyl iodide to afford cationic polyelectrolyte-grafted MWNTs

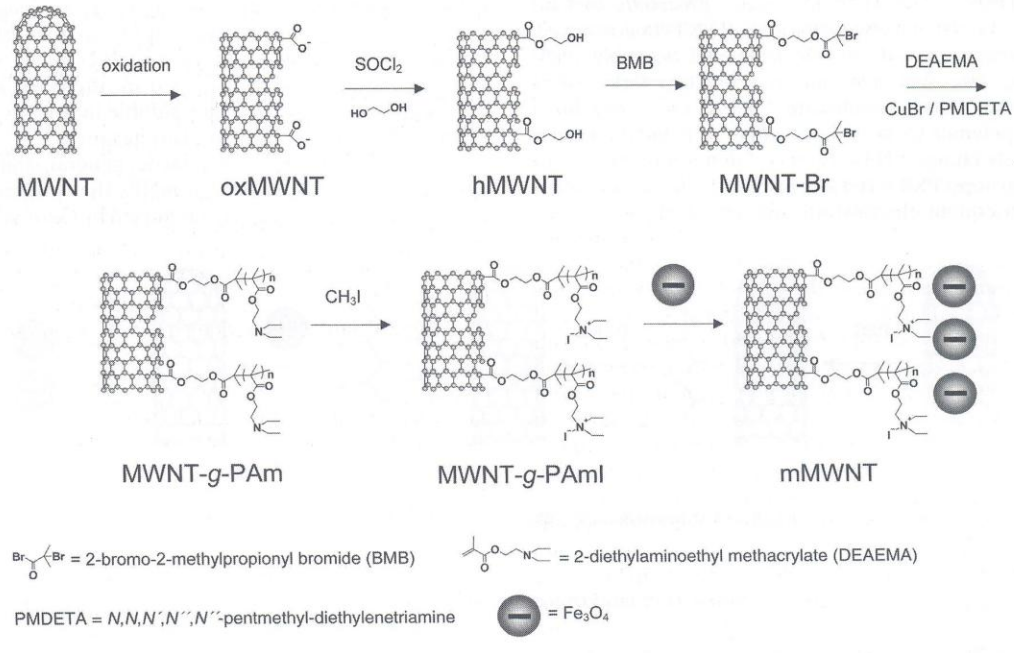

Figure 20. Decoration of polyelectrolyte-coated MWNTs with magnetic nanoparticles [131].

(MWNT-*g*-PAmI). Finally, anionic magnetic iron oxide (Fe_3O_4) NPs were loaded onto the MWNT surfaces by electrostatic assembly between the cationic polyelectrolyte-grafted MWNTs and MNPs to produce supramolecular mMWNTs.

The authors analyzed each step of the procedure by several techniques. The chemical structure of the MWNT-*g*-PAm was confirmed with Fourier transform infrared resonance (FTIR) and hydrogen nuclear magnetic resonance (^{1}H NMR) measurements, while its morphology was observed with high-resolution transmission electron microscopy (HRTEM) and scanning electron microscope (SEM). The crystalline structure of the resulting supramolecular mMWNTs was confirmed with powder X-ray diffraction (XRD) measurements and HRTEM. HRTEM images indicated that the attached mNPs were still crystalline since the crystal lattice was clearly observed. The components and their distributions of the resulting magnetic NTs were assayed by energy-dispersive spectrum (EDS) and elemental mapping analyses. Magnetic properties measurement demonstrated that the obtained magnetic tubes are paramagnetic (same as the iron oxide NPs), and the higher the concentration of loaded NPs, the greater the magnetic density.

To demonstrate an application in bioengineering, single-object technology, and biomedical therapy, the authors used the magnetic tubes as a magnetic handle to manipulate blood cells in a magnetic field. Blood cells attached to mMWNTs could be selectively rotated or transported in a magnetic field.

3. FILLED CARBON NTs

After the first comprehensive and detailed characterization by Iijima [8] and bulk synthesis by Ebbesen and Ajayan [133], MWNTs rapidly became the subject of great enthusiasm and extensive study by academic scientists in several fields. Among these studies, was the filling of the inner cavities of MWNTs with various elements or compounds, primarily in an attempt to produce nanowires [134, 135]. Several theoretical studies had suggested that the introduction of foreign material into the cavities of NTs would enhance or modify the properties of the resulting composites [136–140]. Tube cavities in arc-produced MWNTs are typically in the range of 10–50 nm. Young–Laplace equations predicted that any liquid having a surface tension below approximately 200 mN m^{-1} could spontaneously enter the inner cavity at atmospheric pressure through an open end [141, 142]. However, liquids exhibiting higher surface tensions, such as most molten "heavy" metals, would not be able to fill these cavities unless a suitable pressure difference at the liquid–vapor interface was applied, such as that owing to the low-pressure conditions found in the NTs before opening [143].

The unexpected discovery of SWNT produced a worldwide interest in them as true *nanoobjects* with a diameter more than an order of magnitude smaller than those of MWNTs. In 1998 Smith *et al.* [144] and Sloan *et al.* [155] reported the first examples of SWNTs filled with fullerenes and Ru crystals, respectively. Their results led to the new research field of filled SWNT hybrid nanomaterials that were expected to have novel properties derived from the nanometric dimensions associated with the filled SWNTs. At this level, interaction phenomena are driven by physics, and many physical features that are valid for macroscopic materials can be drastically modified on this nanometric scale. This is particularly true for SWNTs, since the inner diameter of a MWNT is often much larger than that typical of a SWNT.

One of the main goals of filling SWNTs is to force the filler(s) to adopt one-dimensional morphology. Therefore, either the NT acts as a template, which is subsequently removed to obtain a carbon shell–free nanowire for use in the electronic industry since the continuous miniaturization of electronic devices needs nanowires for the contacts or the NT is maintained to give a hybrid material with modified physical properties.

3.1. Materials Encapsulated into Carbon NTs

To date, materials encapsulated in MWNTs and SWNTs are single elements (mainly heavy metals), halides, oxides, hydroxides, phosphides, molecules (mainly fullerenes), and bulk NPs.

The first material inserted into MWNTs was lead although Ajayan and Iijima were not able to determine whether the filling was pure metal or a compound formed by the reaction of lead with carbon and oxygen [134]. They observed that less than about 1% of the tubes were filled. Since then, MWNTs have been primarily filled with single elements (Ag, Au [146], Ge [147], S [147], Sb [147], Se [147, 148], Ru [149], Ni [150], Ni–Pt [150], and Fe [151]) most often by means of a two-step process in which a compound such as a metallic salt was first inserted and then reduced to the free metal by heat treatment in an hydrogen atmosphere. MWNTs were also filled with halides (AuCl [146]), phosphides (Ni–Fe–P and Fe–Co–P [152]), and bulk NPs (fluorescent [153] and paramagnetic iron oxide [154]).

The first material inserted within SWNTs was $RuCl_3$, which was subsequently reduced to metallic Ru by heating in gaseous hydrogen [155]. Other heavy metal elements encapsulated in SWNT are Bi [155], Co [155–157], Fe [157], Ho [157], Gd [157], Ag [158–160], Au [160], Pt [160], and Pd [160]. Halides that were introduced into SWNT are $(KCl)_x$-$(UCl_4)_y$ [158], $AgCl_xBr_y$ [158], $CdCl_2$ [161], $TbCl_3$ [161], TiCl [162], PbI_2 [162], the lanthanide halide $LnCl_3$ [163], KI [161, 164–166], $ZrCl_4$ [167], and $AgCl_xI_{1-x}$ [168]. Oxides introduced into SWNTs include CrO_3 [169] and Sb_2O_3 [161, 170, 171]. Hydroxides introduced into SWNTs include KOH [172], CsOH [172, 173], and $Ba(OH)_2$ [173]. Smith *et al.* [144] reported the first example of SWNTs filled with fullerenes (peapods) as a by-product of the purification and annealing of SWNTs produced by pulsed laser vaporization (PLV). Controlled synthesis of such peapods has been achieved since 2000 [174–179]. Endofullerenes

(fullerenes encapsulating foreign atoms) have also been encapsulated in SWNT ($Gd@C_{82}$ [177, 178, 180–182], $Dy@C_{82}$ [178], $La@C_{82}$ [183], $La_2@C_{82}$ [183], and $Sm@C_{82}$ [183].

3.2. Characterization of Materials Encapsulated into Carbon NTs

The characterization of filled NTs, especially of SWNTs, created numerous technical challenges. In fact, the unambiguous chemical characterization of filled SWNTs remains one of the major issues in the synthesis of filled-SWNT hybrid nanomaterials. For example localized chemical identification by nanoprobe spectroscopic methods on isolated and individual SWNTs may be required to conclude that the foreign material has filled the NTs and is not entangled within bundled NTs. Few complete characterizations have been reported in the literature and these are usually based on TEM images. However, the latter can lack robustness because they often show limited portions of the NTs and filling within bundles instead of isolated individual NTs. Because all scattered electrons are collected, TEM cannot be used to identify elements. Nanoprobe X-ray energy-dispersive spectroscopy (XEDS) may not provide a sufficiently unambiguous identification of the filler as it can identify elements present in the field but not their chemical state. The quantification of filling efficiency is another problem. Recently developed bulk methods based on Raman spectroscopy [184] or electron energy loss spectroscopy (EELS) [181] offer interesting perspectives. In particular, the latter, by being able to count only the inelastically scattered electrons that are characterized by element-specific energy loss, can identify individual elements. By means of EELS, Suenaga *et al.* [181] demonstrated the presence of Gd atoms inside a single chain of endofullerenes within SWNTs.

3.3. Filling Procedures

The most commonly used NT-filling procedures may be classified into three groups that depend on whether the foreign material is inserted by gas phase diffusion (and its related catalytic method), liquid phase capillarity, and solution phase (molten salt) capillarity. A fourth possible procedure was suggested from computer modeling [185], and then realized by Jeong *et al.* [186], and is based on collisions of accelerated atoms on SWNTs. This procedure is also used for filling fullerenes with metal and other atoms.

3.3.1. Filling Rates

A high filling rate has not yet been achieved yet using solids except for fullerene peapods. The latter have mainly been prepared using gas phase diffusion to provide filling rates very close to 100% [180]. Liquid phase capillarity provides maximum filling yields in the range of 20–50%, whereas solution phase capillarity provides no higher yields than 25–30%. The higher filling rates produced by gas phase diffusion can be explained as follows. In general, molecules have to enter the NT *via* openings, a process that may be facilitated by gas phase diffusion in which the NT is first subjected to a dynamic vacuum process that is likely to remove from the NT obstructing molecules or atoms. On contrast, in liquid or solution phase procedure, the filler must enter an unemptied NT that was probably opened by oxidation that could leave impurities that obstruct the openings or produce a solvating shell that reduces filling efficiency. After their removal, solvent molecules encapsulating the foreign material leave empty spaces in the NT cavities. Thus, the reported filling rates of approximately 30% could represent the actual limit for liquid and solution phase techniques. Of course if multiple cycles were performed, higher filling rates may occur, but a filling rate of 100% is unlikely. Even if liquid phase methods provide filling rates intermediate between those obtained by the gas phase and solution-chemistry methods, limitations will occur. Heating in an ampoule under vacuum does not remove residual catalysts from NTs as no previous opening treatment is performed. Furthermore, a limitation of the liquid phase method is that many elements selected for encapsulation in NTs exhibit such very high surface tensions in the molten state that their insertion must be accomplished as salts [145, 146, 158, 159, 163–165]. Removal of the anions by hydrogenation or photolytic reduction inevitably promotes shrinkage of the filler, thereby decreasing the filling yield. However, although the gas phase method appears the most promising, the applicable materials are limited (mainly peapods).

3.3.2. Carbon NT Opening

Whatever the filling method, the first requirement is to open the NT. Liu *et al.* were the first to report an acid-based multireactant opening procedure assisted by cross-flow filtration and sonication that yielded open-ended short (200–300 nm) NTs, which were termed pipes [18]. Other reports provide evidence that NT opening is a side effect of various acid-based purification procedures [158]. Most of these procedures are based on acids such as HCl, HNO_3, H_2SO_4, HNO_3–H_2SO_4, and/or other oxidizing reactants such as H_2O_2 that produce various number of opened NTs. Most purification procedures remove contaminants in as-produced commercial NTs, which have been classified as carbonaceous (amorphous carbon, polyaromatic shells, and graphite particles) and metallic (typically from transition metal catalysts used in their synthesis). However, all NT opening thus far reported have been techniques insufficient to ensure high filling yields. Other treatments were necessary to clean the NT surface, which was found to be partially covered with residual amorphous carbon [147, 157] that blocked the NT openings. Additional treatments included acid or heat under dynamic vacuum. Purification of SWNTs can be found in other chapters of the encyclopedia.

3.3.3. Gas Phase Diffusion and Catalytic Process

Gas Phase Diffusion and Peapods The easiest method to fill NTs with molecular species is by gas phase diffusion in a sealed glass ampoule. Specifically, a mixture of the NTs (which have been opened by an oxidative acid treatment) and the material to be inserted is heated under vacuum at a temperature higher than the filler's sublimation temperature. This technique was found to be particularly successful in encapsulating fullerenes [174–179] and endofullerenes

[177–183] because of their relatively low sublimation temperature, which for fullerenes is approximately 350°C, and their exceptional thermal stability (approximately 3000–4000 K). This technique permits filling yields up to 100%. The gas phase diffusion technique can be used to encapsulate other materials. Brown *et al.* [167] were the first to introduce $ZrCl_4$ into NTs followed by *in situ* clustering by electron beam irradiation within a field emission gun transmission electron microscope (FEGTEM).

The first example of encapsulization of fullerenes in SWNTs (peapods) was reported by Smith *et al.* [144] as a by-product that spontaneously formed during the purification and annealing of raw SWNTs produced by the PLV method. The controlled synthesis of peapods from opened SWNTs that were vacuum annealed in the presence of added fullerenes was reported by both Smith *et al.* [174, 175] and Kataura *et al.* [176]. Smith *et al.* hypothesized that the fullerenes entered the SWNTs through their opened ends and/or imperfections on their sidewalls and then self-assembled into Van der Waals-interacting chains. They showed that on prolonged exposure to an electron beam the encapsulated fullerenes coalesced to form pairs of nested graphene cylinders. They also reported that fullerenes were able to diffuse into SWNTs after their incapsulization [187].

Encapsulation of fullerenes and endofullerenes into SWNTs could have applications in nanoelectronics. The band structure of a SWNT is predicted to be modulated by its encapsulated fullerenes [177]. Similarly, encapsulation of endofullerenes into SWNTs could also alter NT electronic properties differently because endofullerenes and fullerenes have different electronic properties. Shimada *et al.* [177–179] reported the fabrication and characterization of field effect transistors (FETs) of various peapods composed by fullerenes (C_{60}, C_{78}, and C_{90}) and endofullerenes ($Gd@C_{82}$, $Dy@C_{82}$, etc.). Their results suggested that the transfer characteristic could be controlled by selecting the encapsulated endofullerene. However, they first only achieved a low yield of peapod FETs because the peapods were preliminary soot that was dispersed in an organic solvent, then dropped onto a SiO_2–Si substrate with electrodes [177, 178]. Subsequently, they developed a fabrication process in which the peapods were synthesized directly on the substrate similarly to NTs on FETs [179]. This reliable fabrication process permitted them to characterize peapod FETs in detail and obtain a better substrate for future nanoelectronic applications.

Catalytic Process The catalytic method has been used to fill NTs with the gas phase of a material introduced as a cocatalyst during NT synthesis. NTs are typically synthesized while the filler material is sublimed during the electric arc process. An early example of this technique was reported by Kiang *et al.* [155], who used graphite anodes doped with both Co and Bi to obtain single-crystal nanowires of nanometer dimensions. This technique was later used to fill NTs with elements such as Ru [149], Ni [150], Ni–Pt [150], Fe [151], and Co [156].

Considerable interest in preparing well-ordered aligned NT arrays and altering their electronic properties *via* doping or infiltration exists. Dickey *et al.* [149] reported the synthesis of aligned Ru-containing MWNT arrays that exhibited green luminescence and, therefore, potential use in optoelectronic devices. Their synthetic procedure was based on the production of aligned MWNTs using a floating catalyst chemical vapor deposition (CVD) technique [183]. The authors used a mixture of Ru and Fe as the catalyst for MWNT growth on the basis that Ru(II) complexes were widely used as photosensitizers for photochemical conversion, and Ru and Fe have a wide range of solid solubility. The most important feature of this route was that Ru is easily incorporated in NTs during their growth, more precisely in the residual Fe catalyst particles in NTs, thereby eliminating the cumbersome task of ex situ doping or infiltration (as in liquid and solution phase methods). TEM images revealed that the NTs had catalyst particles on the NT root ends, and also on most of their tips. Most NTs also had catalyst inclusions within the tube cores. These structural characteristics indicate that NTs grew by a root-growth mechanism with open tips at the growth front. The HRTEM images and electron diffraction patterns of the catalyst particles at different locations (root ends, cores, and tips) showed that the catalyst existed as single crystals of face-centered cubic Fe. The photoluminescence spectrum of filled MWNTs exhibited a broad intense emission peak at 515 nm that confirmed the presence of Ru inside the NTs. This synthesis method can be readily extended to other transition-metal and rare-earth elements by introducing the appropriate precursor in the synthesis chamber. Potentially, the emission spectrum can be tailored by the choice of elemental precursors and processing conditions that would dictate the particle size. Moreover, CVD-derived MWNT arrays can be selectively grown on patterned substrates that enable the fabrication of nanometer-scale optoelectronic devices.

The sequential catalytic growth (SCG) process allows the synthesis of NTs having regularly spaced NPs encapsulated along their entire length ("carbon nanobulbs") [189]. The SCG mechanism is based on periodic initiation and interruption of NT growth using phosphorous as the catalyst, which induces a kinetic mismatch between carbon supply and consumption. Catalyst NPs were found regularly encapsulated regularly at each new initiation with their spacing dependent on their size and carbon supply. Jourdain *et al.* [152] used SGG process to grow MWNTs containing regularly spaced NPs that were ferromagnetic at room temperature. Specifically, the authors used Fe–Co phosphides which had more favorable ferromagnetic properties than other metal phosphides at room temperature. Their TEM images showed MWNTs with periodic "matchstick" morphology, which is a characteristic of the SCG process [189]. The end of each "match" was filled by an ellipsoidal NP whose volume was a fraction of that of the primary catalyst NP. The authors observed that a typical SCG NT had the following characteristics: (1) sequential encapsulation of more than 100 NPs, (2) slow decrease in both size and separation of the encapsulated NPs along the NT length, and (3) 25–100 nm ellipsoidal length of the NP having the same symmetry axis as the NT and 10–60 nm NP width perpendicular to the MWNT symmetry axis. The encapsulated NPs had saturation magnetization close to that expected for bulk metal phosphides of the same structure and composition, namely $(Fe_{1-x}, M_x)_y P$, where M = Ni or Co, x comprised between 0 and 1, and $y = 2$ or 3. Compared with previous methods, SCG allows encapsulation along

the entire MWNT length and regularly spaced ferromagnetic NPs of well-defined sizes and shapes. Since the periodicity of the NPs was directly correlated directly with the instantaneous growth conditions, SCG is also important for achieving a high degree of structural control over the final composite structure.

3.3.4. Liquid and Solution Phase Capillarity

Sloan *et al.* [145] reported the first inclusion of a 1D nanowire of Ru metal in SWNTs using solution phase capillarity. The filling procedure consisted of (1) opening SWNTs by concentrated HCl, (2) immersing the SWNTs in saturated $RuCl_3$, and (3) reducing the encapsulated $RuCl_3$ by heating in a H_2 atmosphere. The acidification step was required to open the tips of SWNTs. The filling yield was 2–5%. Subsequently, the authors showed that SWNTs could be filled in high yield by the liquid phase method with molten mixtures of silver halides or mixtures of alkali and actinide halides [158]. This procedure was analogous to the solution phase (molten salt) capillary-filling method used to fill MWNTs that was first reported by Ajayan and Iijima [134] and consisted of (1) mixing the anhydrous halide with as-produced (pristine) SWNTs in a silica ampoule that was sealed under vacuum, (2) heating the mixture above the melting point of the halide, and (3) cooling. Foreign (molten) materials could be incorporated into SWNTs if they (1) could wet the capillaries by having surface tensions below a threshold value as determined by Ebbesen [186], (2) had an overall melting temperature that avoided thermal damage to the NTs, and (3) did not chemically attack the NTs.

The Effects of Capillary Confinement Both liquid and solution phase capillary-filling techniques were used to insert halides into the cavities of SWNTs. The size of SWNTs on the crystallization of encapsulated molten binary species produced structures with reduced (or modified) coordination or even novel coordination and stereochemistry. These modifications arose from the restriction of the filler material to a few (2–3) atomic layers in cross section that resulted in structures in which many layers of coordinating ions were missing [165]. Therefore, the capillary confinement forced the filler to have a coordination structure that was profoundly different than the bulk material. Sloan *et al.* [163–168] reported several studies on the impact of the capillary confinement on the low-dimensional crystallization properties of various halides. This topic is further discussed by Goodman *et al.* [190].

3.4. NTs Filled with Bulk NPs

Recently, two groups reported the filling of MWNTs with bulk luminescent and magnetic NPs using capillary suction. Even without the nanometer scale of filled SWNTs, the resulting materials represent useful building blocks for complex NT-based supramolecular nanosystems.

Kim *et al.* [153] experimentally and theoretically studied filling NTs with luminescent NPs (Fig. 21). NTs were synthesized by CVD of carbon on the walls of porous alumina membranes followed by dissolving the alumina in aqueous NaOH. The NTs were collected and suspended in isopropanol, placed on glass cover slips with the aid of dielectrophoresis, and dried. A microdroplet containing (nominal) 50 nm diameter luminescent polystyrene NP was placed at one end of the NPs using a glass micropipette with a 50 μm diameter opening. The filling of the NT by the suspension by capillary action was monitored by optical and luminescent microscopy. The latter showed that luminescent light first occurred at the down-stream end of the NT and propagated upstream along the entire NT length.

The filling process was explained by the authors as the combined action of capillary forces and evaporation. The empty NT was filled initially with a low-density NP suspension by capillary action. At this point the particle concentration was too low for luminescence to be visible through the NT wall by the camera normally used in

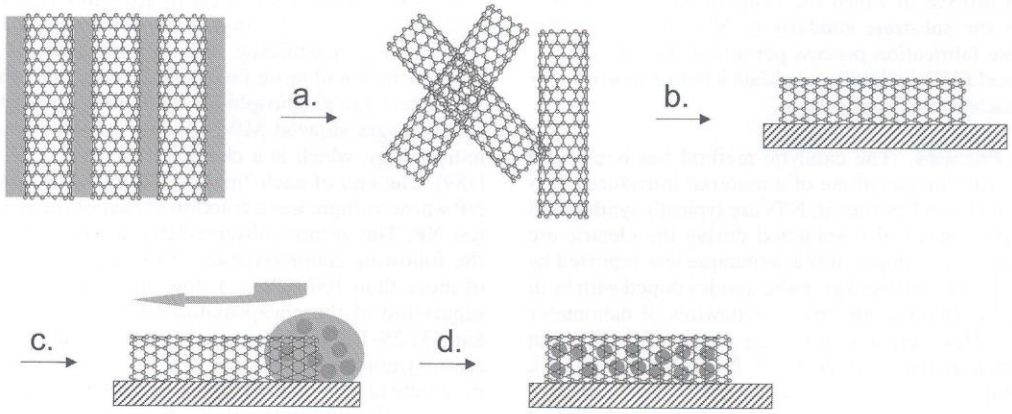

Figure 21. Filling of MWNTs with luminescent NPs [153]. (a) MWNTs were synthesized by CVD of carbon on the walls of porous alumina membranes followed by dissolving the alumina in aqueous NaOH. (b) The NTs were suspended in isopropanol, placed on glass cover slips with the aid of dielectrophoresis and dried. (c) A microdroplet containing luminescent polystyrene NPs was placed at one end of the NTs using a glass micropipette. (d) The filling of the NTs by the luminescent NPs was monitored by optical and luminescent microscopy.

commercially available luminenscent microscopes. During the filling process and thereafter, as front end of the liquid column evaporated, its space was replaced by capillary action with more NP-containing liquid. This process induced a continuous flow of the suspension from the drop into the NT and resulted in an increased NP concentration in comparison with the evaporating surface. A dense aggregate of NPs was formed at the downstream end of the NT and, as the process continued, the aggregate proceeded to form along the length of the NT. The aggregate emitted luminenscent light of a sufficiently high intensity to be readily visible through the NT wall. From these results, the authors concluded that (1) NPs can diffuse along the NT, (2) NTs can be filled with NPs, (3) the filling process can be reasonably predicted with continuum theories, (4) the thin walls of NTs are transparent to luminescent light, and (5) the polymer-based NP inside the NTs can be observed using an electron microscope. As mentioned above, controlled filling of NTs with NPs allowed the modification of the tube properties. In the work reported by Kim *et al.*, luminescent NP-filled NTs were luminenscent in the visible range. In addition, the tubes were also filled with ferromagnetic NPs, endowing them with magnetic properties.

Korneva *et al.* [154] reported a relatively simple, inexpensive, reproducible, scalable, and fast method of filling MWNTs with paramagnetic iron oxide NPs (mNPs) having approximately 10 nm diameter. This technique, which was based on the phenomenon of spontaneous penetration of wetting fluids into capillaries, involved (1) synthesis of MWNTs by the method of noncatalytic CVD in the pores of an alumina template, which provides tubes with open ends free of ferromagnetic catalyst NPs; (2) filling of NTs with mNP suspensions; and (3) separation of NTs from the alumina membrane. The authors also reported a protocol in which the third step preceded the second. These procedures are depicted in Figure 22. In the first method, the alumina membrane with adhering NTs produced by CVD was brought into contact with the mNP suspension. The mNPs entered the membrane pores; on drying only mNPs remained inside the NTs. On dissolving the alumina membrane in aqueous NaOH only magnetic NTs remained. In the second method, the alumina membrane with NTs produced by CVD was dissolved in aqueous NaOH to give the individual NTs. Droplets of a mNP dispersion were then deposited onto NTs to fill. Evaporation of the liquid produced the mNP-filled NTs. Both approaches yielded NTs filled with mNPs. Suspended in liquids, magnetic NTs can follow changes in the direction of applied magnetic field. For example, magnetic NTs can be oriented in the plane of a silicon wafer using gold electrodes or can be forced to stand on the wafer surface. Controllable manipulation of magnetic NTs with micromagnets points to a straightforward way for using these nanoneedles in nanofluidic and electronic devices. Moreover, the versatile technique reported by the authors provides a step toward the nanoengineering of NT-based complex multifunctional nanosystems.

4. CONCLUSIONS

In this chapter, we addressed the supramolecular decoration of both the outer and inner sidewalls of NTs. Since their discovery, NTs have demonstrated the potential to make major contributions to a variety of nanotechnology applications, including, nanomedicine, molecular electronics, fuel cells, hydrogen storage media, and scanning probe microscope tips. NTs can be expected to provide a basis for the future generation of nanoscale devices, and it has been predicted that decoration of their inner or outer sidewalls will lead to an even more diverse range of applications in many fields. For example, while the electrical properties of pristine SWNTs are extremely sensitive to their structure and the existence of defects, which imposes obstacles for their use in electronic device applications, NP-decorated

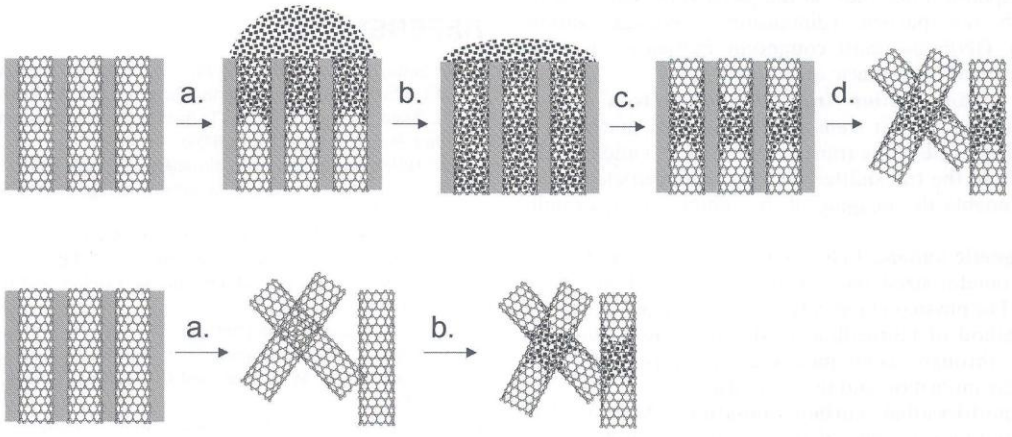

Figure 22. Filling of MWNTs with paramagnetic NPs through capillary forces [154]. Upper panel: (a) the alumina membrane with adhering MWNTs was brought into contact with the magnetic NP suspension; (b) the NPs entered the membrane pores; (c) the fluid was dried to leave only NPs inside NTs and (d) the alumina membrane was dissolved in NaOH to produce NP-filled NTs. Lower panel: (a) the alumina membrane with MWNTs was dissolved in aqueous NaOH and (b) droplets of magnetic NP dispersion were deposited onto NTs. Evaporation of the liquid-produced NP-filled NTs.

SWNTs should be more robust for nanoelectronic applications. While NT-based nanohybrid assemblies will pave the way for the future nanoelectronic uses, difficulties with the chemical characterization of their coating or filling materials have hindered the direct determination of the physical (e.g., transport) properties of single, isolated hybrid SWNTs. Lack of characterization may likely be one of the major issues in the field of SWNT-based hybrid assemblies for the coming years. Thus, besides the technical difficulties of handling and conveniently positioning an approximately 1 nm wide filament onto appropriately sized electrodes, fabricating coated or filled individual NTs, spatially controlling the foreign material on or in the NT sidewall, and ascertaining the actual presence of the foreign material in the portion of the tube being investigated remain necessary and unresolved challenges.

ACKNOWLEDGMENT

We thank Dr. Ana Miletic Sedy (Burnham Institute for Medical Research, La Jolla, CA) for helpful comments.

GLOSSARY

AFM, atomic force microscope The atomic force microscope is a type of scanning probe microscope with sub-nanometer resolution and consisting of a microscale cantilever with a sharp tip at its end which scans the sample. It is used for imaging as well as force spectroscopy measurements.

FRET, fluorescence resonance energy transfer The fluorescence (or Förster) resonance energy transfer is a mechanism describing the energy transfer between two luminophores (the donor and the acceptor) in proximity (less than 10 nm) through non-radiative dipole-dipole coupling.

GNP, gold nanoparticle Gold nanoparticles (also known as colloidal gold) are submicrometer-sized particles that form a stable suspension in aqueous solutions. The color of a GNP suspension depends on the physico-chemical properties of the nanoparticles (dimension, shape, aggregation state, etc). GNPs are most commonly fabricated through the reduction of chloroauric acid.

HRTEM, high-resolution transmission electron microscope High-resolution transmission electron microscope is an imaging mode of the transmission electron microscope that uses both the transmitted and the scattered electronic beams to enable the imaging of the sample at the atomic scale.

mNP, magnetic nanoparticle A magnetic nanoparticle is a submicrometer-sized particle that consists of magnetic elements. The physico-chemical properties of a mNP depend on the method of fabrication. mNPs are most commonly fabricated through techniques such as co-precipitation, thermal decomposition and microemulsion.

MWNT, multi-walled carbon nanutube Multi-walled carbon nanotubes are one of the two structural classes of carbon nanotubes and are formed by several concentric and nested graphene sheets.

NP, nanoparticle A nanoparticle is a portion of matter that behaves as a unit in terms of its physico-chemical properties.

NT, carbon nanotube A carbon nanotube is a tubular structure that belongs to the family of fullerenes. A NT can be thought of as a graphene sheet rolled into a cylinder with a diameter in the order of few nanometers and a length that can be up to several microns.

oxNT, oxidized carbon nanotube Oxidized carbon nanotubes are commonly obtained by treatment of pristine (nonfunctionalized) carbon nanotubes in strong acids in order to functionalize the tube sidewalls with chemical groups that ameliorate the solubility of the nanotubes in aqueous environments and enable further steps of functionalization.

pNT, pristine carbon nanotube A pristine carbon nanotube is a nonfunctionalized carbon nanotube.

QD, quantum dot A quantum dot is a nanometer-sized semiconductor particle characterized by particular electronic properties due to quantum confinement in all the three spatial directions.

SNP, silica nanoparticle Silica nanoparticles are submicrometer-sized particles that are fabricated through hydrolysis and condensation of a silica precursor by wet-chemical techniques.

Str, streptavidin Streptavidin is a tetrameric protein that is widely used in molecular biology (and in several other scientific fields) because of its strong affinity for biotin (vitamin H).

SWNT, single-walled carbon nanotube Single-walled carbon nanotubes are one of the two structural classes of carbon nanotubes and are formed by a single graphene sheet.

TEM, transmission electron microscope A transmission electron microscope uses the transmission of a beam of electrons through the sample to enable the imaging of the sample at a significantly higher resolution than light microscopes.

XPS, X-ray photoelectron spectroscopy X-ray photoelectron spectroscopy is a technique that measures the surface chemical properties (elemental composition, chemical state, etc) of a sample through the analysis of the electrons emitted from the sample irradiated with a beam of X-rays.

REFERENCES

1. R. Saito, G. Dresselhaus, and M. S. Dresselhaus, "Physical Properties of Carbon Nanotubes," London: Imperial College Press, 1999.
2. X. Zhao, Y. Liu, S. Inoue, T. Suzuki, R. O. Jones, and Y. Ando, *Phys. Rev. Lett.* 92, 125502 (2004).
3. M. Hillert and N. Lange, *Z. Kristallogr.* 111, 24 (1958).
4. P. Schützenberger and L. C. R. Schützenberger, *Acad. Sci. Paris* 111, 774 (1890).
5. C. Pélabon and H. C. R. Pélabon, *Acad. Sci. Paris* 137, 706 (1903).
6. A. Oberlin and M. Endo, *J. Cryst. Growth* 32, 335 (1976).
7. M. Audier, A. Oberlin, M. Oberlin, M. Coulon, and L. Bonnetain, *Carbon* 19, 217 (1981).
8. S. Iijima, *Nature* 354, 56 (1991).
9. V. Ellis, K. Vijayamohanan, R. Goswami, N. Chakrapani, L. S. Ramanathan, P. M. Ajayan, and G. Ramanath, *Nano Lett.* 3, 279 (2003).
10. S. Fullam, D. Cottell, H. Rensmo, and D. Fitzmaurice, *Adv. Mater.* 12, 1430 (2000).
11. R. J. Chen, Y. Zhang, D. Wang, and H. J. Dai, *J. Am. Chem. Soc.* 123, 3838 (2001).
12. Y. Tomonari, H. Murakami, and N. Nakashima, *Chemistry* 12, 4027 (2006).

13. H. Paloniemi, T. Ääritalo, T. Laiho, H. Liuke, N. Kocharova, K. Haapakka, F. Terzi, R. Seeber, and J. Lukkari, *J. Phys. Chem. B* 109, 8634 (2005).
14. Y.-Y. Ou and M. H. Huang, *J. Phys. Chem. B* 110, 2031 (2006).
15. Z. Zhong, S. Patskovskyy, P. Bouvrette, J. H. T. Luong, and A. Gedanken, *J. Phys. Chem. B* 108, 4046 (2004).
16. L. Liu, T. Wang, J. Li, Z.-X. Guo, L. Dai, D. Zhang, and D. Zhu, *Chem. Phys. Lett.* 367, 747 (2003).
17. P. Corio, S. D. M. Brown, A. Marucci, M. A. Pimenta, K. Kneipp, G. Dresselhaus, and M. S. Dresselhaus, *Phys. Rev. B* 61, 13202 (2001).
18. J. Liu, A. G. Rinzler, H. Dai, J. H. Hafner, R. K. Bradley, P. J. Boul, A. Lu, *et al.*, *Science* 280, 1253 (1998).
19. K. Jiang, A. Eitan, L. S. Schadler, P. M. Ajayan, R. W. Siegel, N. Grobert, M. Mayne, M. Reyes-Reyes, H. Terrones, and M. Terrones, *Nano Lett.* 3, 275 (2003).
20. B. Kim and W. M. Sigmund, *Langmuir* 20, 8239 (2004).
21. D. I. Gittins and F. Caruso, *Angew. Chem. Int. Ed.* 40, 3001 (2001).
22. S. Hermans, J. Sloan, D. S. Shephard, B. F. G. Johnson, and M. L. H. Green, *Chem. Commun.* 276 (2002).
23. T. Matsumoto, T. Komatsu, K. Arai, T. Yamazaki, M. Kijima, H. Shimizu, Y. Takasawa, and J. Nakamura, *Chem. Commun.* 840 (2004).
24. W. Li, C. Liang, W. Zhou, J. Qiu, Z. Zhou, G. Sun, and Q. Xin, *J. Phys. Chem. B* 107, 6292 (2003).
25. G. Girishkumar, M. Rettker, R. Underhile, D. Binz, K. Vinodgopal, P. McGinn, and P. Kamat, *Langmuir* 21, 8487 (2005).
26. G. Girishkumar, T. D. Hall, K. Vinodgopal, and P. Kamat, *J. Phys. Chem. B* 110, 107 (2006).
27. J. Prabhuram, T. S. Zhao, Z. K. Tang, R. Chen, and Z. X. Liang, *J. Phys. Chem. B* 110, 5245 (2006).
28. A. Kongkanand, S. Kuwabata, G. Girishkumar, and P. Kamat, *Langmuir* 22, 2392 (2006).
29. B. M. Quinn, C. Dekker, and S. G. Lemay, *J. Am. Chem. Soc.* 127, 6146 (2005).
30. T. M. Day, P. R. Unwin, N. R. Wilson, and J. V. Macpherson, *J. Am. Chem. Soc.* 127, 10639 (2005).
31. H. C. Choi, M. Shim, S. Bangsaruntip, and H. Dai, *J. Am. Chem. Soc.* 124, 9058 (2002).
32. L. Qu and L. Dai, *J. Am. Chem. Soc.* 127, 10806 (2005).
33. Z. Q. Tian, S. P. Jiang, Y. M. Liang, and P. K. Shen, *J. Phys. Chem. B* 110, 5343 (2006).
34. Z. B. Yoon and C. M. Wai, *J. Am. Chem. Soc.* 127, 17174 (2005).
35. X. R. Ye, Y. Lin, and C. M. Wai, *Chem. Commun.* 642 (2003).
36. D. Wang, Z.-C. Li, and L. Chen, *J. Am. Chem. Soc.* 128, 15078 (2006).
37. A. Kongkanand, K. Vinodgopal, S. Kuwabata, and P. V. Kamat, *J. Phys. Chem. B* 110, 16185 (2006).
38. B. Yoon, H. Kim, and C. M. Wai, *Chem. Commun.* 1040 (2003).
39. D. Wang, W. X. Ji, and Z. C. Li, *J. Am. Chem. Soc.* 128, 6556 (2006).
40. R. F. Heck and J. P. Nolley, *J. Org. Chem.* 37, 2320 (1972).
41. L. Han, W. Wu, F. L. Kirk, J. Luo, M. M. Maye, N. N. Kariuki, Y. Lin, C. Wang, and C.-J. Zhong, *Langmuir* 20, 6019 (2004).
42. B. Xue, P. Chen, Q. Hong, J. Lin, and K. L. Tan, *J. Mater. Chem.* 11, 2378 (2001).
43. H.-S. Kim, H. Lee, K.-S. Han, J.-H. Kim, M.-S. Song, M.-S. Park, J.-Y. Lee, and J.-K. Kang, *J. Phys. Chem. B* 109, 8983 (2005).
44. G. Che, B. B. Lakshmi, E. R. Fisher, and C. R. Martin, *Nature* 393, 346 (1998).
45. S. H. Joo, S. J. Choi, I. Oh, J. Kwak, Z. Liu, O. Terasaki, and R. Ryoo, *Nature* 412, 169 (2001).
46. S. D. Thompson, L. R. Jordan, and M. Forsyth, *Electrochim. Acta* 46, 1657 (2001).
47. J. Kong, M. G. Chapline, and H. Dai, *Adv. Mater.* 13, 1384 (2001).
48. Y. Lu, J. Li, J. Han. H.-T. Ng, C. Binder, C. Partridge, and M. Meyyappan, *Chem. Phys. Lett.* 391, 344 (2004).
49. D. W. Kim, J. S. Lee, G. S. Lee, L. Overzet, M. Kozlov, A. E. Aliev, Y. W. Park, and D. J. Yang, *J. Nanosci. Nanotechnol.* 6, 3608 (2006).
50. S. Qiaocui, P. Tuzhi, Z. Yunu, and C. F. Yang, *Electroanalysis* 17, 857 (2005).
51. N. Zhu, Z. Chang, P. He, and Y. Fang, *Anal. Chim. Acta* 545, 21 (2005).
52. L. E. Brus, *J. Chem. Phys.* 80, 4403 (1984).
53. L. E. Brus, *Appl. Phys. A* 53, 465 (1991).
54. A. P. Alivisatos, *Science* 271, 933 (1996).
55. A. I. Ekimov, F. Hache, M. C. Schanne-Klein, D. Ricard, C. Flytzanis, I. A. Kudryavtsev, T. V. Yazeva, A. V. Rodina, and Al. L. Efros, *J. Opt. Soc. Am. B* 10, 100 (1993).
56. D. J. Norris and M. G. Bawendi, *Phys. Rev. B* 53, 16338 (1996).
57. Al. L. Efros, M. Rosen, M. Kuno, M. Nirmal, D. J. Norris, and M. Bawendi, *Phys. Rev. B* 54, 4843 (1996).
58. J.-B. Xia, *Phys. Rev. B* 40, 8500 (1989).
59. Al. L. Efros, *Phys. Rev. B* 46, 7448 (1992).
60. E. Martin, C. Delerue, G. Allan, and M. Lannoo, *Phys. Rev. B* 50, 18258 (1994).
61. K. Leung, S. Pokrant, and K. B. Whaley, *Phys. Rev. B* 57, 12291 (1998).
62. L.-W. Wang and A. Zunger, *Phys. Rev. B* 53, 9579 (1996).
63. S. A. McDonald, G. Konstantatos, S. Zhang, P. W. Cyr, E. J. Klem, L. Levina, and E. H. Sargent, *Nat. Mater.* 4, 138 (2005).
64. S. Coe, W. K. Woo, M. Bawendi, and V. Bulovic, *Nature* 420, 800 (2002).
65. W. C. W. Chan and S. M. Nie, *Science* 281, 2016 (1998).
66. M. J. O'Connell, S. M. Bachilo, C. B. Huffman, V. C. Moore, M. S. Strano, E. H. Haroz, K. L. Rialon, *et al.*, *Science* 297, 593 (2002).
67. D. A. Tsybuolski, S. M. Bachilo, and R. B. Weisman, *Nano Lett.* 5, 975 (2005).
68. P. W. Barone, S. Baik, D. A. Heller, and M. S. Strano, *Nat. Mater.* 4, 86 (2004).
69. N. W. Kam, M. J. O'Connell, J. A. Wisdom, and H. Dai, *Proc. Natl. Acad. Sci. USA* 102, 11600 (2005).
70. M. Jones, C. Engtrakul, W. K. Metzger, R. J. Ellingson, A. J. Nozik, M. J. Heben, and G. Rumbles, *Phys. Rev. B* 71, 115426 (2005).
71. W. C. W. Chan, D. J. Maxwell, X. Gao, R. E. Bailey, M. Han, and S. Nie, *Curr. Opin. Biotechnol.* 13, 40 (2002).
72. C. B. Murray, D. J. Norris, and M. G. Bawendi, *J. Am. Chem. Soc.* 115, 8706 (1993).
73. B. O. Dabbousi, J. Rodriguez-Viejo, F. V. Mikulec, J. R. Heine, H. Mattoussi, R. Ober, K. F. Jensen, and M. G. Bawendi, *J. Phys. Chem. B* 101, 9463 (1997).
74. B. Pan, D. Cui, R. He, F. Gao, and Y. Zhang, *Chem. Phys. Lett.* 417, 419 (2006).
75. S. Banerjee and S. S. Wong, *Nano Lett.* 2, 195 (2002).
76. J. M. Haremza, M. A. Hahn, and T. D. Krauss, *Nano Lett.* 2, 1253 (2002).
77. S. Ravidran, S. Chaudhary, B. Colburn, M. Ozkan, and C. S. Ozkan, *Nano Lett.* 3, 447 (2003).
78. M. A. Pimenta, A. Jorio, S. D. M. Brown, A. G. Souza Filho, G. Dresselhaus, J. H. Hafner, C. M. Lieber, R. Saito, and M. S. Dresselhaus, *Phys. Rev. B* 64, 41401 (2001).
79. S. D. M. Brown, A. Jorio, M. S. Dresselhaus, and G. Dresselhaus, *Phys. Rev. B* 64, 73403 (2001).
80. D. B. Mawhinney, V. Naumenko, A. Kuznetsova, J. T. Yates Jr., J. Liu, and R. E. Smalley, *Chem. Phys. Lett.* 324, 213 (2000).
81. H. Hu, P. Bhowmik, B. Zhao, M. A. Hamon, M. E. Itkis, and R. C. Haddon, *Chem. Phys. Lett.* 345, 25 (2001).
82. H. Dumortier, S. Lacotte, G. Pastorin, R. Marega, W. Wu, D. Bonifazi, J.-P. Briand, M. Prato, S. Muller, and A. Bianco, *Nano Lett.* 6, 1522 (2006).
83. M. Bottini, S. Bruckner, K. Nika, N. Bottini, S. Bellucci, A. Magrini, A. Bergamaschi, and T. Mustelin, *Toxicol. Lett.* 160, 121 (2006).

84. C. M. Sayes, F. Liang, J. L. Hudson, J. Mendez, W. Guo, J. M. Beach, V. C. Moore, *et al.*, *Toxicol. Lett*. 161, 135 (2006).
85. D. Cui, F. Tian, C. S. Ozkan, M. Wang, and H. Gao, *Toxicol. Lett*. 155, 73 (2005).
86. S. Fiorito, A. Serafino, F. Andreola, A. Togna, and G. Togna, *J. Nanosci. Nanotechnol.* 6, 591 (2006).
87. C. M. Sayes, A. M. Gobin, K. D. Ausman, J. Mendez, J. L. West, and V. L. Colvin, *Biomaterials* 26, 7587 (2005).
88. A. M. Derfus, W. C. W. Chan, and S. N. Bhatia, *Nano Lett*. 4, 11 (2004).
89. C. M. Goodman, C. D. McCusker, T. Yilmaz, and V. M. Rotello, *Bioconj. Chem*. 15, 897 (2004).
90. M. S. Strano, V. C. Moore, M. K. Miller, M. J. Allen, E. H. Haroz, C. Kittrell, R. H. Hauge, and R. E. Smalley, *J. Nanosci. Nanotechnol.* 3, 81 (2003).
91. S. Chaudhary, J. H. Kim, K. V. Singh, and M. Ozkan, *Nano Lett*. 4, 2415 (2004).
92. M. Olek, T. Büsgen, M. Hilgendorff, and M. Giersig, *J. Phys. Chem. B* 110, 12901 (2006).
93. M. Bottini, A. Magrini, N. Rosato, A. Bergamaschi, and T. Mustelin, *J. Phys. Chem. B* 110, 13685 (2006).
94. M. Bottini, A. Magrini, M. I. Dawson, N. Rosato, A. Bergamaschi, and T. Mustelin, *Carbon* 45, 673 (2007).
95. V. V. Didenko and D. S. Baskini, *Biotechniques* 40, 295 (2006).
96. A. J. Gross and I. W. Sizer, *J. Biol. Chem.* 234, 1611 (1959).
97. L. Qu, R. B. Martin, W. Huang, K. Fu, D. Zweifel, Y. Lin, Y.-P. Sun, *et al.*, *J. Chem. Phys*. 117, 8089 (2002).
98. W. Zhu, N. Minami, S. Kazaoui, and Y. Kim, J. *Mater. Chem.* 13, 2196 (2003).
99. M. Hazani, R. Naaman, F. Hennrich, and M. M. Kappes, *Nano Lett.* 3, 153 (2003).
100. V. Biju, T. Itoh, Y. Baba, and M. Ishikawa, *J. Phys. Chem. B* 110, 26068 (2006).
101. C. A. Dyke and J. M. Tour, *J. Am. Chem. Soc*. 125, 1156 (2003).
102. C. A. Dyke and J. M. Tour, *Nano Lett*. 3, 1215 (2003).
103. P. Roux, P. Jeanteur, and M. Piechaczyk, *Proc. Natl. Acad. Sci. USA* 86, 9079 (1989).
104. F. Balavoine, P. Schultz, C. Richard, V. Mallouh, T. W. Ebbesen, and C. Mioskowski, *Angew. Chem. Int. Ed*. 38, 1912 (1999).
105. J. S. Lenihan, V. G. Gavalas, J. Wang, R. Andrews, and L G. J. Bachas, *J. Nanosci. Nanotechnol.* 4, 600 (2004).
106. N. W. S. Kam and H. Dai, *J. Am. Chem. Soc*. 127, 6021 (2005).
107. M. Bottini, F. Cerignoli, L. Tautz, N. Rosato, A. Bergamaschi, and T. Mustelin, *J. Nanosci. Nanotechnol.* 6, 3693 (2006).
108. M. Bottini, F. Cerignoli, M. I. Dawson, A. Magrini, N. Rosato, and T. Mustelin, *Biomacromolecules* 7, 2259 (2006).
109. D. M. Guldi, G. M. A. Rahman, V. Sgobba, N. A. Kotov, D. Bonifazi, and M. Prato, *J. Am. Chem. Soc*. 128, 2315 (2006).
110. Q. Li, B. Sun, I. A. Kinloch, D. Zhi, H. Sirringhaus, and A. H. Windle, *Chem. Mater.* 18, 164 (2006).
111. S. Banerjee and S. S. Wong, *Chem. Commun*. 1866 (2004).
112. S. Banerjee and S. S. Wong, *J. Am. Chem. Soc*. 125, 10342 (2003).
113. H. Kim and W. Sigmund, *Appl. Phys. Lett.* 81, 2085 (2002).
114. H. Kim and W. Sigmund, *J. Cryst. Growth* 255, 114 (2003).
115. B. Liu and J. Y. Lee, *J. Phys. Chem. B* 109, 23783 (2005).
116. I. Robel, B. A. Bunker, and P. V. Kamat, *Adv. Mater*. 17, 2458 (2005).
117. C. Li, Y. Tang, K. Yao, F. Zhou, Q. Ma, H. Lin, M. Tao, and J. Liang, *Carbon* 44, 2021 (2006).
118. J. Du, L. Fu, Z. Liu, B. Han, Z. Li, Y. Liu, Z. Sun, and D. Zhu, *J. Phys. Chem. B* 109, 12772 (2005).
119. W.-Q. Han and A. Zettl, *Nano Lett*. 3, 681 (2003).
120. S. Lee and W.M. Sigmund, *Chem. Commun*. 780 (2003).
121. W. Stöber, A. Fink, and E. Bohn, *J. Coll. Interf. Sci.* 26, 62 (1968).
122. R. P. Bagwe, C. Yang, L. R. Hilliard, and W. Tan, *Langmuir* 20, 8336 (2004).
123. M. Bottini, L. Tautz, H. Huynh, E. Monosov, N. Bottini, M. I. Dawson, S. Bellucci, and T. Mustelin, *Chem. Commun.* 758 (2005).
124. M. Bottini, A. Magrini, M. I. Dawson, A. Bergamaschi, and T. Mustelin, *Carbon* 44, 1298 (2006).
125. M. Bottini, A. Magrini, A. Di Venere, S. Bellucci, M. I. Dawson, N. Rosato, A. Bergamaschi, and T. Mustelin, *J. Nanosci. Nanotechnol.* 6, 1381 (2006).
126. J. Liu, M. J. Casavant, M. Cox, D. A. Walters, P. Boul, W. Lu, A. J. Rimberg, K. A. Smith, D. T. Colbert, and R. E. Smalley, *Chem. Phys. Lett.* 303, 125 (1999).
127. Q. Fu, C. Lu, and J. Liu, *Nano Lett*. 2, 329 (2002).
128. R. Zanella, E. V. Basiuk, P. Santiago, V. A. Basiuk, E. Mireles I. Puente-Lee, and J. M. Saniger, *J. Phys. Chem. B* 109, 16290 (2005).
129. M. A. Correa-Duarte, M. Grzelczak, V. Salgueiriño-Maceira, M. Giersig, L. M. Liz-Marzán, M. Farle, K. Sierazdki, and R. Diaz, *J. Phys. Chem. B* 109, 19060 (2005).
130. V. Georgakilas, V. Tzitzios, D. Gournis, and D. Petridis, *Chem. Mater.* 17, 1613 (2005).
131. C. Gao, W. Li, H. Morimoto, Y. Nagaoka, and T. Maekawa, *J. Phys. Chem. B* 110, 7213 (2006).
132. H. Kong, C. Gao, and D. Yan, *Macromolecules* 37, 4022 (2004).
133. T. W. Ebbesen and P. M. Ajayan, *Nature* 357, 365 (1992).
134. P. M. Ajayan and S. Iijima, *Nature* 361, 333 (1993).
135. S. C. Tsang, Y. K. Chen, J. F. Harris, and M. L. H. Green, *Nature* 372, 159 (1994).
136. M. S. Dresselhaus, *Nature* 358, 195 (1992).
137. J. W. Mintmire, B. I. Dunlap, and C. T. White, *Phys. Rev. Lett*. 68, 631 (1992).
138. R. Saito, M. Fujita, G. Dresselhaus, and M. S. Dresselhaus, *Mater. Sci. Eng. B* 19, 185 (1993).
139. D. Östling, D. Tománek, and A. Rosén, *Phys. Rev. B* 55, 13980 (1997).
140. F. J. García-Vidal, J. M. Pitarke, and J. B. Pendry, *Phys. Rev. B* 58, 6783 (1998).
141. M. R. Pederson and J. Q. Broughton, *Phys. Rev. Lett.* 69, 2689 (1992).
142. E. Dujardin, T. W. Ebbesen, H. Hiura, and K. Taginaki, *Science* 265, 1850 (1994).
143. P. M. Ajayan, T. W. Ebbesen, T. Ichihashi, S. Iijima, K. Tanigaki, and H. Hiura, *Nature* 362, 522 (1993).
144. B. W. Smith, M. Monthioux, and D. E. Luzzi, *Nature* 396, 323 (1998).
145. J. Sloan, J. Hammer, M. Zwiefka-Sibley, and M. L. H. Green, *Chem. Commun*. 347 (1998).
146. A. Chu, J. Cook, R. J. R. Heesom, J. L. Hutchison, M. L. H. Green, and J. Sloan, *Chem. Mater*. 8, 2751 (1996).
147. A. Loiseau and H. Pascard, *Chem. Phys. Lett*. 256, 246 (1996).
148. J. Chancolon, F. Archaimbault, A. Pineau, and S. Bonnamy, *J. Nanosci. Nanotechnol*. 6, 82 (2006).
149. E. C. Dickey, C. A. Grimes, M. K. Jain, K. G. Ong, D. Qian, P. D. Kichambare, R. Andrews, and D. Jacques, *Appl. Phys. Lett.* 79, 4022 (2001).
150. M. K. Singh, E. Titus, P. K. Tyagi, U. Palnitkar, D. S. Misra, M. Roy, A. K. Dua, C. S. Cojocaru, and F. Le Normand, *J. Nanosci. Nanotechnol.* 3, 165 (2003).
151. S. Hampel, A. Leonhardt, D. Selbmann, K. Biedermann, D.Elefant, Ch. Müller, T. Gemming, and B. Büchner, *Carbon* 44, 2316 (2006).
152. V. Jourdain, E. T. Simpson, M. Paillet, T. Kasama, R. E. Dunin-Borkowski, P. Poncharal, A. Zahab, A. Loiseau, J. Robertson, and P. Bernier, *J. Phys. Chem. B* 110, 9759 (2006).
153. B. M. Kim, S. Qian, and H. H. Bau, *Nano Lett*. 5, 873 (2005).
154. G. Korneva, H. Ye, Y. Gogotsi, D. Halverson, G. Friedman, J.-C. Bradley, and K. G. Kornev, *Nano Lett*. 5, 879 (2005).
155. C. H. Kiang, J. S. Choi, T. T. Tran, A. D. Bacher, *J. Phys. Chem. B* 103, 7449 (1999).
156. S. Liu, J. Zhu, Y. Mastai, I. Felner, and A. Gedanken, *Chem. Mater.* 12, 2205 (2000).

157. B. C. Satishkumar, A. Taubert, and D. E. Luzzi, *J. Nanosci. Nanotechnol.* 3, 159 (2003).
158. J. Sloan, D. M. Wright, H. G. Woo, S. Bailey, G. Brown, A. P. E. York, K. S. Coleman, J. L. Hutchinson, and M. L. H. Green, *Chem. Commun*. 699 (1999).
159. Z. L. Zhang, B. Li, Z. J. Shi, Z. N. Gu, Z. Q. Xue, and L. M. Peng, *J. Mater. Res.* 15, 2658 (2000).
160. A. Govindaraj, B. C. Satishkumar, M. Nath, and C. N. R. Tao, *Chem. Mater.* 12, 202 (2000).
161. J. Sloan, S. Friedrichs, E. Flahaut, G. Brown, S. R. Bailey, K. S. Coleman, C. Xu *et al.*, in "Electronic Properties of Molecular Nanostructures" (H. Kuzmany, J. Fink, M. Mehring, and S. Roth S, Eds.), Vol. 591, p. 277, American Institute of Physics Conference Proceedings Series, 2001.
162. E. Flahaut, J. Sloan, K. S. Coleman, and M. L. H. Green, in "Electronic Properties of Molecular Nanostructures" (H. Kuzmany, J. Fink, M. Mehring, and S. Roth S, Eds.), Vol. 591, p. 283, American Institute of Physics Conference Proceedings Series, 2001.
163. C. Xu, J. Sloan, G. Brown, S. Bailey, V. C. Williams, S. Friedrichs, K. S. Coleman, *et al.*, *Chem. Commun.* 2427 (2000).
164. J. Sloan, M. C. Novotny, S. R. Bailey, G. Brown, C. Xu, V. C. Williams, S. Friedrichs, *et al.*, *Chem. Phys. Lett.* 329, 61 (2000).
165. R. R. Meyer, J. Sloan, R. E. Dunin-Borkowski, A. Kirkland, M. C. Novotny, S. R. Bailey, J. L. Hutchison, and M. L. H. Green, *Science* 289, 1324 (2000).
166. M. Wilson and P. A. Madden, *J. Am. Chem. Soc*. 123, 2101 (2001).
167. G. Brown, S. Bailey, J. Sloan, C. Xu, S. Friedrichs, E. Flahaut, K. S. Coleman, J. L. Hutchison, R. E. Dunin-Borkowski, and M. L. H. Green, *Chem. Commun*. 845 (2001).
168. J. Sloan, M. Terrones, S. Nufer, S. Friedrichs, S. R. Bailey, H.-G. Woo, M. Rühle, J. L. Hutchison, and M. L. H. Green, *J. Am. Chem. Soc*. 124, 2116 (2002).
169. J. Mittal, M. Monthioux, H. Allouche, and O. Stephan, *Chem. Phys. Lett.* 339, 311 (2001).
170. S. Friedrichs, R. R. Meyer, J. Sloan, A. I. Kirkland, J. L. Hutchison, and M. L. H. Green, *Chem. Commun*. 929 (2001).
171. S. Friedrichs, J. Sloan, M. L. H. Green, J. L. Hutchison, R. R. Meyer, and A. I. Kirkland, *Phys. Rev. B* 64, 45406 (2001).
172. N. Thamavaranukup, H. A. Höppe, L. Ruiz-Gonzalez, P. M. F. J. Costa, J. Sloan, A. Kirkland, and M. L. H. Green, *Chem. Commun.* 1686 (2004).
173. L. Shao, G. Tobias, Y. Huh, and M. L. H. Green, *Carbon* 44, 2849 (2006).
174. B. W. Smith and D. E. Luzzi, *Chem. Phys.* Lett. 321, 169 (2000).
175. D. E. Luzzi and B. W. Smith, *Carbon* 38, 1751 (2000).
176. H. Kataura, Y. Maniwa, T. Kodama, K. Kikuchi, K. Hirahara, K. Suenaga, S. Iijima, S. Suzuki, Y. Achiba, and W. Krätschmer, *Synth. Metals* 121, 1195 (2001).
177. T. Shimada, T. Okazaki, R. Taniguchi, T. Sugai, H. Shinohara, K. Suenaga, Y. Ohno, S. Mizuno, S. Kishimoto, and T. Mizutani, *Appl. Phys. Lett.* 81, 4067 (2002).
178. T. Shimada, Y. Ohno, T. Okazaki, T. Sugai, K. Suenaga, S. Kishimoto, T. Mizutani, *et al.*, *Physica E* 21, 1089 (2004).
179. Y. Ohno, Y. Kurokawa, S. Kishimoto, T. Mizutani, T. Shimada, M. Ishida, T. Okazaki, *et al.*, *Appl. Phys. Lett.* 86, 23109 (2005).
180. K. Hirahara, K. Suenaga, S. Bandow, H. Kato, T. Okazaki, H. Shinohara, and S. Iijima, *Phys. Rev. Lett.* 85, 5384 (2000).
181. K. Suenaga, M. Tence, C. Mory, C. Colliex, H. Kato, T. Okazaki, H. Shinohara, K. Hirahara, S. Bandow, and S. Iijima, *Science* 290, 2280 (2000).
182. J. Lee, H. Kim, S.-J. Kahng, G. Kim, Y.-W. Son, J. Ihm, H. Kato, *et al.*, *Nature* 415, 1005 (2002).
183. K. Suenaga, K. Hirahara, S. Bandow, S. Iijima, T. Okazaki, H. Kato, and H. Shinohara, in "Electronic Properties of Molecular Nanostructures" (H. Kuzmany, J. Fink, M. Mehring, and S. Roth S, Eds.), Vol. 591, p. 256, American Institute of Physics Conference Proceedings Series (2001).
184. H. Kataura, Y. Maniwa, T. Kodama, K. Kikuchi, K. Hirahara, S. Iijima, S. Suzuki, W. Krätschmer, and Y. Achiba, in "Electronic Properties of Molecular Nanostructures" (H. Kuzmany, J. Fink, M. Mehring, and S. Roth S, Eds.), Vol. 591, p. 251, American Institute of Physics Conference Proceedings Series, 2001.
185. A. A. Farajian, K. Ohno, K. Esfarjani, Y. Maruyama, and Y. Kawazoe, *J. Chem. Phys.* 111, 2164 (1999).
186. G.-H. Jeong, R. Hatakeyama, T. Hirata, K. Tohji, K. Motomiya, T. Yaguchi, and Y. Kawazoe, *Chem. Commun.* 152 (2003).
187. B. W. Smith, M. Monthioux, and D. E. Luzzi, *Chem. Phys. Lett* 315, 31 (1999).
188. R. Andrews, D. Jacques, A. M. Rao, F. Derbyshire, D. Qian, X. Fan, E. C. Dickey, and J. Chen, *Chem. Phys. Lett* 303, 467 (1999).
189. Z. P. Zhu, D. S. Su, Y. Lu, R. Schlögl, G. Weinberg, and Z. Y. Liu, *Adv. Mater*. 16, 447 (2004).
190. J. Sloan, A. I. Kirkland, J. L. Hutchison, and M. L. H. Green, *Chem. Commun*. 1319 (2002).